

Forced-unfolding and force-quench refolding of RNA hairpins

Changbong Hyeon¹ and D. Thirumalai^{1,2*}

¹*Biophysics Program*

Institute for Physical Science and Technology

²*Department of Chemistry and Biochemistry*

University of Maryland,

College Park, MD 20742

(Dated: October 28, 2018)

Abstract

Nanomanipulation of individual RNA molecules, using laser optical tweezers, has made it possible to infer the major features of their energy landscape. Time dependent mechanical unfolding trajectories, measured at a constant stretching force (f_S), of simple RNA structures (hairpins and three helix junctions) sandwiched between RNA/DNA hybrid handles show that they unfold in a reversible all-or-none manner. In order to provide a molecular interpretation of the experiments we use a general coarse-grained off-lattice Go-like model, in which each nucleotide is represented using three interaction sites. Using coarse-grained model we have explored forced-unfolding of RNA hairpin as a function of f_S and the loading rate (r_f). The simulations and theoretical analysis have been done without and with the handles that are explicitly modeled by semiflexible polymer chains. The mechanisms and time scales for denaturation by temperature jump and mechanical unfolding are vastly different. The directed perturbation of the native state by f_S results in a sequential unfolding of the hairpin starting from their ends whereas thermal denaturation occurs stochastically. From the dependence of the unfolding rates on r_f and f_S we show that the position of the unfolding transition state (TS) is not a constant but moves dramatically as either r_f or f_S is changed. The TS movements are interpreted by adopting the Hammond postulate for forced-unfolding. Forced-unfolding simulations of RNA, with handles attached to the two ends, show that the value of the unfolding force increases (especially at high pulling speeds) as the length of the handles increases. The pathways for refolding of RNA from stretched initial conformation, upon quenching f_S to the quench force f_Q , are highly heterogeneous. The refolding times, upon force quench, are at least an order of magnitude greater than those obtained by temperature quench. The long f_Q -dependent refolding times starting from fully stretched states are analyzed using a model that accounts for the microscopic steps in the rate limiting step which involves the trans to gauche transitions of the dihedral angles in the GAAA tetraloop. The simulations with explicit molecular model for the handles show that the dynamics of force-quench refolding is strongly dependent on the interplay of their contour length and the persistence length, and the RNA persistence length. Using the generality of our results we also make a number of precise experimentally testable predictions.

*Corresponding author phone: 301-405-4803; fax: 301-314-9404; thirum@glue.umd.edu

INTRODUCTION

RNA molecules adopt precisely defined three dimensional structures in order to perform specific functions [1]. To reveal the folding pathways navigated by RNA en route to their native conformations requires exhaustive exploration of the complex underlying energy landscape over a wide range of external conditions. In recent years, mechanical force has been used to probe the unfolding of a number of RNA molecules [2, 3, 4]. Force is a novel way of probing regions of the energy landscape that cannot be accessed by conventional methods (temperature changes or variations in counterion concentrations). In addition, response of RNA to force is relevant in a number of cellular processes such as mRNA translocation through the ribosome and the activity of RNA-dependent RNA polymerases. Indeed, many dynamical processes are controlled by deformation of biomolecules by mechanical force.

By exploiting the ability of single molecule laser optical tweezer (LOT) to control the magnitude of the applied force Bustamante and coworkers have generated mechanical unfolding trajectories for RNA hairpins and *Tetrahymena thermophila* ribozyme [5, 6]. The unfolding of the ribozyme shows multiple routes with great heterogeneity in the unfolding pathways [6]. In their first study [5] they showed that simple RNA constructs (P5ab RNA hairpins or a three helix junction) unfold reversibly at equilibrium. From the time traces of the end-to-end distance (R) of P5ab, for a number of force values, Liphardt *et. al.* [5] showed that the hairpins unfold in a two-state manner. The histograms of time dependent R (and assuming ergodicity) were used to calculate the free energy difference between the folded and unfolded states. Unfolding kinetics as a function of the stretching force f_S was used to identify the position of the transition states [5, 7, 8]. These experiments and subsequent studies have established force as a viable way of quantitatively probing the RNA energy landscape with R serving as a suitable reaction coordinate.

The experiments by Bustamante and coworkers have led to a number of theoretical and computational studies using a variety of different methods [9, 10, 11, 12, 13, 14]. These studies have provided additional insights into the mechanical unfolding of RNA hairpins and ribozymes. In this paper we build on our previous work [14] and new theoretical analysis to address a number of questions that pertain to mechanical unfolding of RNA hairpins. In addition, we also provide the first report on force-quench refolding of RNA hairpins. The present paper addresses the following major questions:

- 1) Are there differences in the mechanism of thermal and mechanical unfolding? We expect these two processes to proceed by different pathways because denaturation induced by temperature jump results in a stochastic perturbation of the native state while destabilization by force is due to a directed perturbation. The molecular model for P5GA gives a microscopic picture of these profound differences.
- 2) For a given sequence does the position of the transition state move in response to changes in the loading rate (r_f) or the stretching force f_S ? Based on the analysis of experiments over a narrow range of conditions (fixed temperature and loading rate) it has been suggested that the location of the sequence-dependent unfolding transition state (TS) for secondary structure is midway between the folded state while the TS for the ribozyme is close to the native conformation [5]. Explicit simulations show that the TS moves dramatically especially at high values of f_S and r_f . As a consequence the dependence of the unfolding rate on f_S deviates from the predictions of the Bell model

[15].

- 3) What is the origin of the dramatic differences in refolding by force-quench from stretched conformations and temperature-quench refolding? Experiments by Fernandez and Li [8] on refolding initiated by force-quench on polyubiquitin construct suggest similar differences in the refolding time scales. For RNA hairpins we show that the incompatibility of the local loop structures in the stretched state and the folded conformations lead to extremely long refolding times upon force-quench.
- 4) What are the effects of linker dynamics on forced-unfolding and force-quench refolding of RNA hairpins? The manipulation of RNA is done by attaching a handle or linker to the 3' and 5' ends of RNA. Linkers in the LOT experiments, that are done under near-equilibrium conditions, are RNA/DNA hybrid handles. These are appropriately modeled as worm-like chain (WLC). By adopting an explicit polymer model for semi-flexible chains we show that, under certain circumstance, non-equilibrium response of the handle (which is not relevant for the LOT experiments) can alter the forced-unfolding dynamics of RNA. We probe the effects of varying the linker characteristics on the dynamics of folding/unfolding of RNA for the model of the handle-RNA-handle construct. In certain range of r_f non-equilibrium effects on the dynamics of linkers can affect the force-extension profiles.

METHODS

Hairpin sequence: To probe the dynamics of unfolding and force-quench refolding we have studied in detail the 22-nucleotide hairpin, P5GA whose solution structure has been determined by NMR (Protein Data Bank (PDB) id:1eor). In many respects P5GA is similar to P5ab in the P5abc domain of group I intron [16]. Both these structures have GA mismatches and are characterized by the presence of the GAAA tetraloop. The sequence of P5GA is GGCGAAGUCGAAAGAUGGCGCC [17].

RNA model: Because it is difficult to explore, using all atom models of biomolecules in explicit water, unfolding and refolding of RNA hairpins over a wide range of external conditions (temperature (T), stretching force (f_S), and quench force (f_Q)), we have introduced a minimal off-lattice coarse-grained model [14] (Throughout the paper we use f for referring to mechanical force in general terms while f_S and f_Q have specific meaning). In this model each nucleotide is represented by three beads with interaction sites corresponding to the phosphate (P) group, the ribose (S) group, and the base (B) [14]. Thus, the RNA backbone is reduced to the polymeric structure $[(P - S)_n]$ with the base that is covalently attached to the ribose center. In the minimal model the RNA molecule with N nucleotides corresponds to $3N$ interaction centers. The secondary structure and the lowest energy structure using the minimal model are shown in Fig.1.

Energy function: The total energy of a RNA conformation, that is specified by the coordinates of the $3N$ sites, is written as $V_T = V_{BL} + V_{BA} + V_{DIH} + V_{STACK} + V_{NON} + V_{ELEC}$. Harmonic potentials are used to enforce structural connectivity and backbone rigidity. The

connectivity between two beads ($P_i S_i$, $S_i P_{i+1}$ and $B_i S_i$) is maintained using

$$V_{BL} = \sum_{i=1}^{2N-2} \frac{1}{2} k_r \{ |\vec{r}_{(SP)_{i+1}} - \vec{r}_{(SP)_i}| - (R_{SP}^o)_i \}^2 + \sum_{i=1}^N \frac{1}{2} k_r \{ |\vec{r}_{B_i} - \vec{r}_{S_i}| - (R_{BS}^o)_i \}^2 \quad (1)$$

where $k_r = 20 \text{ kcal}/(\text{mol} \cdot \text{\AA}^2)$, $(R_{SP}^o)_i$ and $(R_{BS}^o)_i$ are the distances between covalently bonded beads in PDB structure. The notation $(SP)_i$, denotes the i^{th} backbone bead S or P . The angle θ formed between three successive beads ($P_i - S_i - P_{i+1}$ or $S_{i-1} - P_i - S_i$) along sugar-phosphate backbone is subject to the bond-angle potential,

$$V_{BA} = \sum_{i=1}^{2N-3} \frac{1}{2} k_\theta (\theta_i - \theta_i^o)^2 \quad (2)$$

where $k_\theta = 20 \text{ kcal}/(\text{mol} \cdot \text{rad}^2)$, and θ_i^o is the value in the PDB structure.

Dihedral angle potential : The dihedral angle potential (V_{DIH}) describes the ease of rotation around the angle formed between four successive beads along the sugar-phosphate backbone ($S_{i-1} P_i S_i P_{i+1}$ or $P_i S_i P_{i+1} S_{i+1}$). The i -th dihedral angle ϕ_i , which is the angle formed between the two planes defined by four successive beads i to $i+3$, is defined by $\cos \phi_i = (\vec{r}_{i+1,i} \times \vec{r}_{i+1,i+2}) \cdot (\vec{r}_{i+2,i+1} \times \vec{r}_{i+2,i+3})$. In the coarse-grained model the right-handed chirality of RNA is realized by appropriate choices of the parameters in the dihedral potential. Based on the angles in the PDB structure (ϕ_i^o), one of the three types of dihedral potentials, *trans* (t , $0 < \phi_i^o < 2\pi/3$), *gauche(+)* (g^+ , $2\pi/3 < \phi_i^o < 4\pi/3$), *gauche(-)* (g^- , $4\pi/3 < \phi_i^o < 2\pi$), is assigned to each of the four successive beads along the backbone. The total dihedral potential of the hairpin is

$$V_{DIH} = \sum_{i=1}^{2N-4} [A_{1i}^\eta + B_{1i}^\eta + C_{1i}^\eta + A_{2i}^\eta \cos(\phi_i - \phi_i^o + \phi_i^\eta) + B_{2i}^\eta \cos 3(\phi_i - \phi_i^o + \phi_i^\eta) + C_{2i}^\eta \sin(\phi_i - \phi_i^o + \phi_i^\eta)] \quad (3)$$

where the parameters (in kcal/mol) defined for t , g^+ , and g^- are

$$A_{1i} = 1.0, A_{2i} = -1.0, B_{1i} = B_{2i} = 1.6, C_{1i} = 2.0, C_{2i} = -2.0 \quad (\eta = g^+),$$

$$A_{1i} = 1.0, A_{2i} = -1.0, B_{1i} = B_{2i} = 1.6, C_{1i} = 2.0, C_{2i} = 2.0 \quad (\eta = g^-),$$

$$A_{1i} = A_{2i} = 1.2, B_{1i} = B_{2i} = 1.2, C_{1i} = C_{2i} = 0.0 \quad (\eta = t).$$

To account for the flexibility in the loop region we reduce the dihedral angle barrier by halving the parameter values in $19 \leq i \leq 24$.

Stacking interactions: Simple RNA secondary structures, such as hairpins, are largely stabilized by stacking interactions whose context dependent values are known [18, 19, 20]. The folded P5GA RNA hairpin is stabilized by nine hydrogen bonds between the base pairs (see Fig.1-B) including two GA mismatch pairs [17]. The stacking interactions that stabilize a hairpin can be written as $V_{STACK} = \sum_{i=1}^{n_{max}} V_i$ ($n_{max} = 8$ in P5GA). We assume that the orientation-dependent V_i is

$$V_i(\{\phi\}, \{\psi\}, \{r\}; T) = \Delta G_i(T) \times e^{-\alpha_{st} \{ \sin^2(\phi_{1i} - \phi_{1i}^o) + \sin^2(\phi_{2i} - \phi_{2i}^o) + \sin^2(\phi_{3i} - \phi_{3i}^o) + \sin^2(\phi_{4i} - \phi_{4i}^o) \}} \times e^{-\beta_{st} \{ (r_{ij} - r_{1i}^o)^2 + (r_{i+1j-1} - r_{2i}^o)^2 \}} \times e^{-\gamma_{st} \{ \sin^2(\psi_{1i} - \psi_{1i}^o) + \sin^2(\psi_{2i} - \psi_{2i}^o) \}} \quad (4)$$

where $\Delta G(T) = \Delta H - T\Delta S$, the bond angles $\{\phi\}$ are $\phi_{1i} \equiv \angle S_i B_i B_j$, $\phi_{2i} \equiv \angle B_i B_j S_j$, $\phi_{3i} \equiv \angle S_{i+1} B_{i+1} B_{j-1}$, $\phi_{4i} \equiv \angle B_{i+1} B_{j-1} S_{j-1}$, the distance between two paired bases $r_{ij} = |B_i - B_j|$, $r_{i+1j-1} = |B_{i+1} - B_{j-1}|$, and ψ_{1i} and ψ_{2i} are the dihedral angles formed by the four beads $B_i S_i S_{i+1} B_{i+1}$ and $B_{j-1} S_{j-1} S_j B_j$, respectively. The superscript o refers to angles and distances in the PDB structure. The values of α_{st} , β_{st} and γ_{st} are 1.0, 0.3\AA^{-2} and 1.0 respectively. We take ΔH and ΔS from Turner's thermodynamic data set [18, 19]. There are no estimates for GA related stacking interactions. Nucleotides G and A do not typically form a stable bond and hence GA pairing is considered a mismatch. We use the energy associated with GU for GA base pair.

Nonbonded interactions: We use the Lennard-Jones interactions between non-bonded interaction centers to account for the hydrophobicity of the purine/pyrimidine groups. The total nonbonded potential is

$$V_{NON} = \sum_{i=1}^{N-1} \sum_{j=i+1}^N V_{B_i B_j}(r) + \sum_{i=1}^N \sum_{m=1}^{2N-1} V'_{B_i (SP)_m}(r) + \sum_{m=1}^{2N-4} \sum_{n=m+3}^{2N-1} V_{(SP)_m (SP)_n}(r) \quad (5)$$

where $r = |\vec{r}_i - \vec{r}_j|$. The prime in the second term on the Eq.(5) denotes the condition $m \neq 2i - 1$. In our model, a native contact exists between two non-covalently bound beads provided they are within a cut-off distance r_c ($=7.0\text{\AA}$). Two beads beyond r_c are considered to be non-native. For a native contact,

$$V_{\xi_i \eta_j}(r) = C_h^{\xi_i \eta_j} \left[\left(\frac{r_{ij}^o}{r} \right)^{12} - 2 \left(\frac{r_{ij}^o}{r} \right)^6 \right] \quad (6)$$

where r_{ij}^o is the distance between beads in PDB structure and $C_h^{\xi_i \eta_j} = 1.5 \text{ kcal/mol}$ for all native contact pairs except for $B_{10} B_{13}$ base pair associated with the formation of the hairpin loop, for which $C_h^{B_{10} B_{13}} = 3.0 \text{ kcal/mol}$. The additional stability for the base pair associated with loop formation is similar to the Turner's thermodynamic rule for the free energy gain in the tetraloop region. For beads beyond r_c the interaction is

$$V_{\xi_i \eta_j}(r) = C_R \left[\left(\frac{a}{r} \right)^{12} + \left(\frac{a}{r} \right)^6 \right] \quad (7)$$

with $a = 3.4\text{\AA}$ and $C_R = 1 \text{ kcal/mol}$. The value of $C_h^{\xi_i \eta_j} (= 1.5 \text{ kcal/mol})$ has been chosen so that the hairpin undergoes a first order transition from unfolded states. Our results are not sensitive to minor variations in C_h .

Electrostatic interactions: The charges on the phosphate groups are efficiently screened by counterions so that in the folded state the destabilizing contribution of the electrostatic potential is relatively small. However, the nature of the RNA conformation (especially tertiary interactions) can be modulated by changing counterions. For simplicity, we assume that the electrostatic potential between the phosphate groups is pairwise additive $V_{ELEC} = \sum_{i=1}^{N-1} \sum_{j=i+1}^N V_{P_i P_j}(r)$. For $V_{P_i P_j}(r)$ we use Debye-Hückel potential, which accounts for screening by condensed counterions and hydration effects, and is given by

$$V_{P_i P_j} = \frac{z_{P_i} z_{P_j} e^2}{4\pi \epsilon_0 \epsilon_r r} e^{-r/l_D} \quad (8)$$

where $z_{P_i} = -1$ is the charge on the phosphate ion, $\epsilon_r = \epsilon/\epsilon_0$ and the Debye length $l_D = \sqrt{\frac{\epsilon_r k_B T}{8\pi k_{elec} e^2 I}}$ with $k_{elec} = \frac{1}{4\pi\epsilon_0} = 8.99 \times 10^9 JmC^{-2}$. To calculate the ionic strength $I = 1/2 \sum_i z_i^2 c_i$, we use the value $c_i = 200mM-NaCl$ from the header of PDB file [17]. We use $\epsilon_r = 10$ in the simulation [21]. Because the Debye screening length $\sim \sqrt{T}$ the strength of electrostatic interactions between the phosphate groups are temperature dependent even when we ignore the variations of ϵ with T . At room temperature ($T \sim 300 K$) the electrostatic repulsion between the phosphate groups at $r \sim 5.8 \text{ \AA}$, which is the closest distance between phosphate groups, is $V_{P_i P_{i+1}} \sim 0.5 \text{ kcal/mol}$. Thus, V_{ELEC} between phosphate groups across the base pairing ($r = 16 \sim 18 \text{ \AA}$) is almost negligible. The Debye-Hückel interactions is most appropriate for monovalent counterions like Na^+ .

Models for linker or “handles”: In laser optical tweezer (LOT) experiments the RNA molecules are attached to the polystyrene beads by an RNA/DNA hybrid handles or linker. A schematic illustration of the pulling simulations that mimic the experimental setups for the laser optical tweezer (LOT) (Fig.2-A) is shown in Fig.2-B. Globally, the principles involved in atomic force microscope (AFM) and LOT for mechanical unfolding of biomolecules are essentially the same except for the difference in the effective spring constant. The spring constant of the nearly harmonic potential of the optical trap is in range $k = 0.01 - 0.1 \text{ pN/nm}$ whereas the cantilever spring in AFM experiments (Fig.2-B) is much stiffer and varies from $1 - 10 \text{ pN/nm}$. To fully characterize the RNA energy landscape it is necessary to explore a wide range of loading rates [22]. To vary r_f we have used different values of k in the simulations.

We simulate mechanical unfolding of RNA hairpins either by applying a constant force on the 3'- end with the 5'- end being fixed (unfolding at constant force), or by pulling the 3'- end through a combination of linkers and harmonic spring (Fig.2-B) at a constant speed in one direction (unfolding at constant loading rate). Comparison of the results allows us to test the role of the linker dynamics on the experimental outcome. If the linker is sufficiently stiff then it should not affect the dynamics of RNA. On the other hand, unfolding at constant loading rate ($r_f \equiv k \times v$, where v is the pulling speed and the stretching force (f_s) is computed using $f = k \times \delta z$ with δz being the displacement of the spring) can be modulated either by changing k or v . Instead of k an effective spring constant k_{eff} , with $k_{eff}^{-1} = k_{eff}^{-1} + k_{linker}^{-1} + k_{mol}^{-1}$, should be used to compute the loading rate. Typically, k_{linker}^{-1} and k_{mol}^{-1} (where k_{mol} is the stiffness associated with the model) are small and, hence $k_{eff} \approx k$. In this setup, the relevant variables are k , v , and the contour length (L) of the linker and the effective stiffness of the linker. We explore the effects of these factors by probing changes in the force extension curve (FEC). The variations in L are explored only using constant loading rate simulations. Manosas and Ritort [13] used an approximate method to model linker dynamics.

The energy function for the linker molecule is

$$V_L = \sum_{i=1}^{N-1} \frac{k_B}{2} (r_{i,i+1} - b)^2 - \sum_{i=1}^{N-2} k_A \hat{r}_{i,i+1} \cdot \hat{r}_{i+1,i+2} \quad (9)$$

where $r_{i,i+1}$ and $\hat{r}_{i,i+1}$ are the distance and unit vector connecting i and $i + 1$ residue, respectively. For the bond potential we set $k_B = 20 \text{ kcal}/(\text{mol} \cdot \text{\AA}^2)$ and $b = 5 \text{ \AA}$. This form of the energy function describes the worm-like chain (WLC) [23] (appropriate for RNA/DNA hybrid handles used by Liphardt *et. al.* [5]) when k_A is large. The linker

becomes more flexible as the parameter describing the bending potential, k_A , is reduced. Thus, by varying k_A the changes in the entropic elasticity of the linker on RNA hairpin dynamics can be examined. We use $k_A = 80 \text{ kcal/mol}$ or 20 kcal/mol to change the flexibility of the linker. For the purpose of computational efficiency, we did not include excluded volume interactions between linkers or between the linker and RNA. When linkers are under tension the chains do not cross unless thermal fluctuations are larger than the energies associated with force. To study the linker effect on force extension curves (FEC), we attach two linker polymers each with the contour length $L/2$ to the ends of the hairpin and stretch the molecule using the single pulling speed $0.86 \times 10^2 \text{ } \mu\text{m/s}$ with spring constant $k = 0.7 \text{ pN/nm}$. The total linker length is varied from $L = (10-50) \text{ nm}$.

Simulations: We assume that the dynamics of the molecules (RNA hairpins and the linkers) can be described by the Langevin equation. The system of Langevin equations is integrated as described before [14, 24]. Using typical values for the mass of a bead in a nucleotide (B_i , S_i or P_i), $m = 100 \text{ g/mol} \sim 160 \text{ g/mol}$, the average distance between the adjacent beads $a = 4.6 \text{ } \text{\AA}$, the energy scale $\epsilon_h = 1 \sim 2 \text{ kcal/mol}$, the natural time is $\tau_L = (\frac{ma^2}{\epsilon_h})^{1/2} = 1.6 \sim 2.8 \text{ ps}$. We use $\tau_L = 2.0 \text{ ps}$ to convert the simulation times into real times. To estimate the time scale for thermal and mechanical unfolding dynamics we use a Brownian dynamics algorithm [25, 26] for which the natural time for the overdamped motion is $\tau_H = \frac{\zeta \epsilon_h}{T} \tau_L$. We use $\zeta = 50 \tau_L^{-1}$, which approximately corresponds to friction constant in water, in the overdamped limit. To probe the thermodynamics and kinetics of folding we used a number of physical quantities (end-to-end distance (R), fraction of native contacts (Q), the structural overlap function (χ), number of hydrogen bonds n_{bond} , etc) to monitor the structural change in the hairpin.

Computation of free energy profiles: We adopted the multiple histogram technique [27, 28] to compute the thermodynamic averages of all the observables at various values of T and f . For example, the thermodynamic average of the fraction of native contact, Q , can be obtained at arbitrary values of T and f if the conformational states are well sampled over a range of T and f values. The thermodynamic average of Q is given by

$$\langle Q(T, f) \rangle = \frac{\sum_{E,R,Q} Q e^{-(E-fR)/T} \frac{\sum_{k=1}^K h_k(E, R, Q)}{\sum_{k=1}^K n_k e^{(F_k - (E-f_k R))/T_k}}}{\sum_{E,R,Q} e^{-(E-fR)/T} \frac{\sum_{k=1}^K h_k(E, R, Q)}{\sum_{k=1}^K n_k e^{(F_k - (E-f_k R))/T_k}}} \equiv \sum_Q Q P[Q(T, f)] \quad (10)$$

where K is the number of histograms, $h_k(E, R, Q)$ is the number of states between E and $E + \delta E$, R and $R + \delta R$, Q and $Q + \delta Q$ in the k -th histogram, $n_k = \sum_{E,R,Q} h_k(E, R, Q)$, T_k and f_k are the temperature and the force in the simulations used to generate the k -th histogram, respectively. The free energy, F_k , that is calculated self-consistently, satisfies

$$e^{-F_r/T_r} = \sum_{E,R,Q} e^{-(E-f_r R)/T_r} \frac{\sum_{k=1}^K h_k(E, R, Q)}{\sum_{k=1}^K n_k e^{(F_k - (E-f_k R))/T_k}}. \quad (11)$$

Using the low friction Langevin dynamics, we sampled the conformational states in the (T, f) in the range $\{0 < K < T < 500 \text{ K}, f = 0.0 \text{ pN}\}$ and $\{0.0 \text{ pN} < f < 20.0 \text{ pN}, T = 305 \text{ K}\}$. Exhaustive samplings around the transition regions at $\{305 \text{ K} \leq T \leq 356 \text{ K}, f = 0.0 \text{ pN}\}$ and $\{5.0 \text{ pN} \leq f \leq 7.0 \text{ pN}, T = 305 \text{ K}\}$ is required to obtain reliable estimates of the

thermodynamic quantities. The free energy profile, with Q as an order parameter, is given by

$$F[Q(T, f)] = F_o(T, f) - k_B T \log P[Q(T, f)]. \quad (12)$$

where $F_o(T, f) = -k_B T \log Z(T, f)$, $Z(T, f) = \sum_{E, R, Q} e^{-(E-fR)/T} \frac{\sum_{k=1}^K h_k(E, R, Q)}{\sum_{k=1}^K n_k e^{(E_k - (E-f_k R))/T_k}}$ and $P[Q(T, f)]$ is defined in Eq.(10). The free energy profile $F(R)$ with R as a reaction coordinate can be obtained using a similar expression.

RESULTS

Mechanisms of thermal denaturation and forced-unfolding are different: We had previously reported [14] the thermodynamic characteristics of the P5GA hairpin as a function of T and f . The native structure of the hairpin, that was determined using a combination of multiple slow cooling, simulated annealing, and steepest descent quench, yielded conformations whose average root mean square deviation (RMSD) with respect to the PDB structure is about 0.1 Å [14]. The use of Go-like model leads to a small value of RMSD. From the equilibrium (T, f) phase diagram in [14] the melting temperature $T_m \approx 341$ K at $f_S = 0$. Just as in thermal denaturation at T_m at zero f the hairpin unfolds by a weak first order transition at an equilibrium critical force f_c . Above f_c , which is a temperature-dependent, the folded state is unstable.

To monitor the pathways explored in the thermal denaturation we initially equilibrated the conformations at $T = 100$ K at which the hairpin is stable. Thermal unfolding ($f = 0$) was initiated by a temperature jump to $T = 346$ K $> T_m$. Similarly, forced-unfolding is induced by applying a constant force $f_S = 42$ pN to thermally equilibrated initial conformation at $T = 254$ K [14]. The value of $f_S = 42$ pN far exceeds $f_c = 15$ pN at $T = 254$ K. Upon thermal denaturation, the nine bonds fluctuate (in time) stochastically in a manner that is independent of one another until the hairpin melts (Fig.3-A). Forced-unfolding, on the other hand, occurs in a directed manner. Mechanical unfolding occurs by sequential unzipping with force unfolding the bond, from the ends of the hairpin (beginning at bond 1) to the loop (Fig.3-B).

The differences in the folding pathways are also mirrored in the free energy profiles. Assuming that Q is an adequate reaction coordinate for thermal unfolding [29] we find, by comparing $F(Q)$ at $T = 100$ K and $T = 346$ K, that thermal melting occurs by crossing a barrier. The native basin of attraction (NBA) at $Q = 0.9$ at $T = 100$ K is unstable at the higher temperature and the new equilibrium at $Q \sim 0.2$ is reached in an apparent two state manner (Fig.3-C). Upon “directed” mechanical unfolding the free energy profile $F(R)$ is tilted from the NBA at $R \approx 1.5$ nm to $R \approx 12$ nm at which the stretched states are favored at $f = 42$ pN. The forced-unfolding transition also occurs abruptly once the activation barrier at $R \approx 1.5$ nm (close to the folded state) is crossed (Fig.3-D).

Free energy profiles and transition state (TS) movements: Based on the proximity of the average transition state location, Δx_F^{TS} , it has been suggested that folded states of RNA [6] and proteins [7] are brittle. If the experiments are performed by stretching at a constant loading rate then Δx_F^{TS} is calculated using $f^* \sim k_B T / \Delta x_F^{TS} \log r_f$ [30] where f^* is the most probable unfolding force and r_f , the loading rate, is $r_f = df/dt = kv$. Substantial curvatures in the dependence of f^* on $\log r_f$ ($[f^*, \log r_f]$ plot) have been observed especially

if r_f is varied over a wide range [22]. Similarly, in constant force unfolding experiments Δx_F^{TS} is obtained from the Bell equation [15] that relates the unfolding rate to the applied force, $\log k_U = \log k_U^o + f\Delta x_F^{TS}/k_B T$ where k_U^o is the unfolding rate in the absence of force. In the presence of curvature in the $[f^*, \log r_f]$ plots or when the Bell relationship is violated [31] it is difficult to extract meaningful values of k_U^o or Δx_F^{TS} by a simple linear extrapolation. By carefully examining the origin of curvature in the $[f^*, \log r_f]$ plot or in k_U as we show that in the unfolding of hairpin the observed non-linearities are due to movements in the transition state ensemble i.e., Δx_F^{TS} depends on f_S and r_f .

Unfolding at constant loading rate: We performed forced unfolding simulations by varying both the pulling speed v and the spring constant k so that a broad range of loading rates can be covered. The unfolding forces at which all the hydrogen bonds are ruptured are broadly distributed with the average and the dispersion that increase with growing loading rates (Fig.4-A). The plot of f^* as a function of $\log r_f$ (Fig.4-B) shows marked departure from linearity. The slope of the plot ($[f^*, \log r_f]$) increases sharply as r_f increases. There are two possible reasons for the increasing tangent. One is the reduction of Δx_F^{TS} , which would lead to an increase in the slope ($k_B T / \Delta x_F^{TS}$) of f^* vs $\log r_f$. The other is the increase of curvature at the transition state region, i.e., barrier top of free energy landscape. Regardless of the precise reason, it is clear that the standard way of estimating Δx_F^{TS} using f^* at large loading rates results in a very small value of Δx_F^{TS} . We estimate Δx_F^{TS} from $[f^*, \log r_f]$ plot to be 4 Å at $r_f \approx 10^5$ pN/s. The estimated value of Δx_F^{TS} is unphysical because 4 Å is less than the average distance between neighboring P atoms. The minimum pulling speed used in our simulations is nearly five orders of magnitude greater than in experiments. The use of large loading rate results in small values of Δx_F^{TS} . If the simulations can be performed at small values of r_f we expect the slope of f^* vs $\log r_f$ to decrease, which would then give rise to physically reasonable values of Δx_F^{TS} at low r_f . Our simulations suggest that the curvature in the plot of f^* as a function of $\log r_f$ is due to the dependence of Δx_F^{TS} on r_f and not due to the presence of multiple transition states [22]. As a result, extrapolation to low r_f values can give erroneous results (Fig.4-B).

Unfolding at constant force: To monitor the transition state movements we performed a number of unfolding simulations by applying $f_S > 20$ pN at $T = 290$ K. The unfolding rates are too slow at $f_S < 20$ pN to be simulated. Nevertheless, the simulations give strong evidence for force-dependent movement of Δx_F^{TS} . For a number of values of f_S in the range 20 pN $< f_S < 150$ pN we computed the distribution of first passage times for unfolding. The first passage time for the i -th molecule is reached if R becomes $R = 5$ nm for the first time. From the distribution of first passage times (for about (50-100) molecules at each f_S) we calculated the mean unfolding time. Just as for unfolding at constant r_f the dependence of $\log \tau_U$ on f_S shows curvature (Fig.5-A), and hence deviates from the often used Bell model [31]. By fitting τ_U to the Bell formula ($\tau_U = \tau_U^o e^{-f_S \Delta x_F^{TS} / k_B T}$), over a narrow range of f_S we obtain $\Delta x_F^{TS} \approx 4$ Å which is too small to be physically meaningful at $f_S = 0$.

Insights into the shift of Δx_F^{TS} as f_S increases can be gleaned from the equilibrium force-dependent free energy $F(R)$ as a function of R . The one-dimensional free energy profiles $F(R)$ show significant movements in Δx_F^{TS} as f_S changes (Fig.5-C). As f_S increases Δx_F^{TS} decreases sharply, which implies that the unfolding TS is close to the folded state. At smaller values of f_S the TS moves away from the native state. At the midpoint of

the transition $\Delta x_F^{TS} \approx 5.5 \text{ nm}$ which is about half-way to the native state. The result for $\Delta x_F^{TS}/R_U \approx 1/2$ (R_U is the average value of R in the unfolded state) is in accord with experiments [5] which were done at forces that are not too far from the equilibrium unfolding force. Although Δx_F^{TS} is dependent on the RNA sequence it is likely that, for simple hairpins $\Delta x_F^{TS}/R_U \approx 1/2$. The prediction that Δx_F^{TS} is dependent on f_S is amenable to experimental test.

Force-quench refolding times depend (approximately) exponentially on f_Q : One of the great advantages of force quench refolding experiments [8] is that the ensemble of conformations with a predetermined value of R can be prepared by suitably adjusting the value of f_S [8]. Because force-quench refolding can be initiated from conformations with arbitrary values of R , regions of the energy landscape that are completely inaccessible in conventional experiments can be probed. In order to initiate refolding by force quench we generated extended conformations with $R = 13.5 \text{ nm}$, using $f_S = 90 \text{ pN}$ at $T = 290 \text{ K}$. Subsequently, we reduced the force to f_Q in the range $0.5 \text{ pN} < f_Q < 4 \text{ pN}$. For these values of f_Q the hairpin conformation is preferentially populated at equilibrium. The probability $P_U(t)$ that the RNA hairpin remains unfolded at six f_Q values decays non-exponentially (Fig.6). The mean refolding times $\tau_F(f_Q)$, upon force quench, that are computed using $P_U(t)$ ($\tau_F = \int_0^\infty t P_U(t) dt$), show that *in the range* $0.5 \text{ pN} < f_Q < 4 \text{ pN}$ (Fig.5-B)

$$\tau_F(f_Q) = \tau_F^o \exp(f_Q \Delta x_U^{TS} / k_B T) \quad (13)$$

where Δx_U^{TS} is the distance from the unfolded basin of attraction to the refolding transition state, and τ_F^o is the refolding time in the absence of force. Linear regression gives $\tau_F^o \approx 290 \mu\text{s}$ and $\Delta x_U^{TS} \approx 1 \text{ nm}$. The value of Δx_U^{TS} , which is obtained from kinetic simulations, is in accord with the location of Δx_U^{TS} obtained directly from the equilibrium free energy profiles $F(R)$ (Fig.5-C). In the $0.5 \text{ pN} < f_Q < 4 \text{ pN}$ range the distance from UBA to the TS is approximately 1 nm and is a constant. Thus, kinetic and thermodynamic data lead to a consistent picture of force-quench refolding.

If the simulations are done with $f_Q \equiv 0 \text{ pN}$ then we find that $\tau_F(f_Q = 0) \approx 191 \mu\text{s}$ (Fig.5-B) which differs from τ_F^o obtained using Eq.(13). When f_Q is set to zero, the 3' end fluctuates whereas when $f_Q \neq 0$ the 3' end remains fixed. The rate limiting step in the hairpin formation is the trans→gauche transitions in the dihedral angles in the GAAA tetraloop region (see below). When one end is free to fluctuate, as is the case when $f_Q = 0$, the trans→gauche occurs more rapidly than $f_Q \neq 0$. The difference between $\tau_F(f_Q = 0)$ and τ_F^o is, perhaps, related to the restriction in the conformational search among the compact structures which occurs when one end of the chain is fixed.

Metastable intermediates lead to a lag phase in the refolding kinetics: The presence of long lived conformations (see below), with several incorrect dihedral angles in the GAAA tetraloop, is also reflected in the refolding kinetics as monitored by $P_U(t)$. If there are parallel routes to the folded state then $P_U(t)$ can be described using a sum of exponentials. The lag kinetics, which is more pronounced as f_Q increases (see especially $f_Q = 4 \text{ pN}$ in Fig.6) can be rationalized using a kinetic scheme $S \xrightarrow{\tau_1} I \xrightarrow{\tau_2} F$ where S is the initial stretched state, I is the intermediate state, and F is the folded hairpin. Setting

$P_U(t) \equiv P_S(t) + P_I(t) = 1 - P_F(t)$, we obtain

$$P_U(t) = \frac{1}{\tau_2 - \tau_1} (\tau_2 e^{-t/\tau_2} - \tau_1 e^{-t/\tau_1}). \quad (14)$$

From Fig.6, which shows the fits of the simulated $P_U(t)$ to Eq.(14), we obtain the parameters (τ_1, τ_2) at each f_Q (see caption to Fig.6 for the values). If folding is initiated by temperature-quench $\tau_1 \ll \tau_2$ so that $P_U(t) \sim e^{-t/\tau_2}$. Explicit simulations show that thermal refolding occurs in a two-state manner (data not shown). In force-quench refolding both τ_1 and τ_2 increase as f_Q increases and $\tau_1/\tau_2 \sim O(1)$ at the higher values of f_Q . There are considerable variations in the structures of the metastable intermediate depending on f_Q . The variations in the conformations are due to the differences in the number of incorrect or non-native dihedral angles. As a consequence there are multiple steps in force quench refolding in contrast to forced-unfolding which occurs in an all-or-none manner.

Trans \rightarrow gauche transitions in the GAAA tetraloop dihedral angles lead to long refolding times: It is of interest to compare the refolding times obtained from stretched ensemble ($\tau_F(f_Q)$) and the refolding time ($\tau_F(T)$) from thermally denatured ensemble. In a previous paper [14], we showed that $\tau_F(f_Q = 0) = 15\tau_F(T)$ (Fig.5-B). The large difference in refolding times may be because the initial conditions from which folding commences are vastly different upon force and temperature quench [14, 32]. The fully stretched conformations, with $R = 13.5 \text{ nm}$, are very unlikely to occur in an equilibrated ensemble even at elevated temperatures. The canonical distribution of thermally denatured conformations even at $T = 1500 \text{ K}$ ($\gg T_F$) shows that the probability of populating conformations with $R = 13.5 \text{ nm}$ (Fig.7-A) is practically zero. Thus, folding from thermally denatured ensemble starts from relatively compact conformations. In contrast, the initial condition for force-quench refolding can begin (as in our simulations) from fully stretched conformations upon force-quench. Both R and the radius of gyration (R_g) undergo substantial changes en route to the NBA. Indeed, the refolding trajectories from extended conformations exhibit broad fluctuations in $R(t)$ in the order of (25-75Å) for long time periods, followed by a cooperative reduction in R at the final stage (Fig.7-B).

The long refolding times upon force-quench starting from fully stretched conformations may be generic for folding of globular proteins as well. Recent experiments on force-quench refolding of poly-ubiquitin (Ub) [8] show that $R(t)$ for proteins exhibit behavior similar to that shown in Fig.7-B. The resulting f_Q -dependent refolding times for poly-Ub (0.1 – 10 sec) are considerably larger compared to τ_F ($\approx 5 \text{ msec}$ [33, 34]) in the absence of force. Because the collapse of a single ubiquitin molecule in solution occurs in less than a millisecond, the origin of the long refolding times has drawn considerable attention [32, 35]. The microscopic model considered here for RNA can be used to shed light on the origin of the generic long refolding times upon force quench.

From the phase diagram (see Fig.(2) in [14]) it is clear that the routes navigated by RNA hairpin upon thermal and force quench have to be distinct. While the distinct initial conditions do not affect the native state stability (as long as the final values of T and f_Q are the same) they can profoundly alter the rates and pathways of folding. The major reason for the long force-quench refolding times in RNA hairpins is that in the initial stretched state there is a severe distortion (compared to its value in the native state) in one of the dihedral angles. The 19-th dihedral angle (found in the GAAA loop region) along the sugar-phosphate backbone is in g^+ conformation in the native state while in the initial stretched

conformation it is in the t state (Fig.8-A). Thus, if all the molecules are in the fully stretched conformation then the 19th dihedral angle in each of them has to, during the force-quench refolding process, undergo the $t \rightarrow g^+$ transition in the GAAA tetraloop region in order to fold. The enthalpic barrier associated with the $t \rightarrow g^+$ transition is about $1k_B T$ (Fig.8-B). However, this transition is coupled to the dynamics in the other degrees of freedom and such a cooperative event (see Fig.7-B for examples of trajectories) makes the effective free energy barrier even higher. Although significant fluctuations are found in thermally denatured ensemble at $T = 500 K$, they are not large enough to produce non-native dihedral angles in the GAAA tetraloop. The dihedral angles in thermally denatured conformations do not deviate significantly from their values in the native conformation (Fig.8-C). In contrast upon fully stretching P5GA dihedral angles in the GAAA tetraloop adopt non-native values (Fig.8-D).

The time scale for the $t \rightarrow g^+$ transitions can be inferred from the individual trajectories. Typically, there are large fluctuations due to $g^+ \leftrightarrow t \leftrightarrow g^-$ transitions in the dihedral angles in the flexible loop region ($i = 19 - 24$). For the trajectory in Fig.9-B we observe the persistence of incorrect dihedral angle in the loop region for $t \sim 300 \mu s$. At $t > 300 \mu s$ the native-like dihedral angles form. Subsequently, the formation and propagation of interaction stabilizing the native RNA hairpin takes place. These dynamical transitions are clearly observed in Figs.9-B and 9-C. The observed mechanism is reminiscent of a nucleation process. We conclude that the formation of the flexible loop with all the dihedral angles achieving near native values is the rate limiting step in the refolding kinetics of RNA hairpins upon force-quench starting from fully stretched state. It should be stressed that the rate limiting step for thermal refolding of P5GA or force-quench refolding starting from partially stretched conformations (see below) is different. The observation that the zipping of the hairpin takes place upon synchronous formation of all the native-like dihedral angles suggests the presence of a high entropic barrier. The crossing of the entropic barrier results in slow refolding if P5GA is fully stretched.

Linker effects on RNA force-extension curves : In LOT experiments the force-extension curves (FECs) are measured for the handle(H)-RNA-handle(H) construct [5, 6]. To unambiguously extract the FEC for RNA alone (from the measured FEC for H-RNA-H construct) the properties of the handle, namely, the contour length L_H and the persistence length l_p^H cannot be chosen arbitrarily. In the experiments by Liphardt *et. al.* $L_H = 320 nm$ and $l_p^H = 50 nm$ for the RNA/DNA hybrid handle. We expect that both $\lambda = l_p^H / l_p^{RNA}$ and l_p^H will affect the FEC curves of the object of interest, namely, the RNA molecule. To discern the signature for the force-induced transition in the RNA hairpin alone from the FEC for H-RNA-H construct λ has to be large. If we assume $l_p^{RNA} \approx 1 nm$ then the experimental value of $\lambda \approx 50$ which is large enough to extract the transitions in the RNA hairpin. If $\lambda \approx 1$ then the entropic fluctuations in the handle can mask the signals in RNA [36]. Similarly the end-to-end distance fluctuation in the handle, δR , should be smaller than the extension in RNA. Because δR grows with L_H (see below) it follows that if very long L_H is used even with $\lambda \gg 1$ the signal from RNA can be masked. The square of the fluctuations in the end-to-end distance δR of the linker is given by $(\delta R)^2 = \partial \langle R \rangle / \partial (\beta f_S)$ where $\langle R \rangle$ is the mean end-to-end distance. For WLC, that describes the linkers, we expect $\langle R \rangle \sim (2L_H l_p)^{1/2}$ for

small f_S and $\langle R \rangle \sim L_H$ for large f_S provided L_H is long. Thus,

$$\delta R \sim \begin{cases} (L_H l_p^H)^{1/4} (k_B T / f_S)^{1/2} & (f_S \lesssim k_B T) \\ L_H^{1/2} (k_B T / f_S)^{1/2} & (f_S \gg k_B T) \end{cases} \quad (15)$$

The mean fluctuation in the extension of the spring is, using equipartition theorem, given by

$$\delta x \sim \sqrt{\frac{k_B T}{k}}. \quad (16)$$

In order for the signal from RNA to be easily discerned from the experimentally measured FEC, the expansion of end-to-end distance of the molecule at transition should be larger than δR and δx . Since δR grows sublinearly with the linker length (Eq.(15)) the attachment of large linker polymer can mask the transition signal. These arguments show the characteristics of the linker can obscure the signals from RNA.

The FECs in the simulations can also be affected by non-equilibrium effects due to the linker dynamics. In the handle(H)-RNA-handle(H) construct considered here the force exerted at one of the linker depends on the angle between f_S and the end of the linker. The initial event in force transmission along the contour of the H-RNA-H construct is the alignment of the molecule along the force direction. The characteristic time for force to reach RNA so that unfolding can occur is f_c / r_f where f_c is the critical force. Non-equilibrium effects due to linker dynamics become relevant if τ_R , the time scale for alignment of H-RNA-H along the force direction, $\tau_R > f_c / r_f$. This condition is not relevant in experiments which are conducted at small values of r_f . However, it is important to consider non-equilibrium effects in simulations which are performed at high r_f values. The characteristic time depends on L_H and l_p^H .

We validate these arguments by obtaining FEC for H-P5GA-H by varying L_H and $\lambda = l_p^H / l_p^{RNA}$. Using the WLC for the linker we calculated FEC where the L_H is varied from (10 – 50) nm. In order to observe rapid unfolding we have carried out our simulation at the pulling speed $v = 0.86 \times 10^2 \mu\text{m}/\text{sec}$ and $k = 0.7 \text{ pN}/\text{nm}$. Under these conditions non-equilibrium effects are relevant for the linker [23] which is not the case in experiments. The FECs show clearly a plateau in the range $20 \text{ pN} < f_S < 40 \text{ pN}$ which corresponds to the two-state hairpin opening (Fig.10). For the experimentally relevant plot (Fig.10-A) that shows FEC for H-P5GA-H the transition plateau is present at all values of L_H . However, when L_H reaches 50 nm the signal from P5GA is masked. The FEC for P5GA alone (Fig.10-B) shows modest increase in the unfolding force as L_H increases. Similarly, we find the value of unfolding force also increases as the linker flexibility increases. These observations are due to non-equilibrium effects on the linker dynamics because of the relatively large values of r_f used in the simulations.

Our simulations show that, at high loading rates, the length of the handle is also important. This issue is not relevant in experiments in which loading rates are much smaller. However, they become important in interpreting simulation results. In our case $r_f (= kv)$ is 6×10^4 times that used in experiments. At such high r_f non-equilibrium effects control the linker dynamics [23]. Thus, to extract unfolding signatures from RNA alone it is necessary to use high value of λ and relatively short values of L . In other words FEC, when r_f is varied, may be a complicated function of l_p^H / l_p^{RNA} and L_H / l_p^H .

Force-quench refolding of P5GA with attached linkers: It is convenient to monitor force-quench refolding of RNA alone using simulations. A similar experiment can only be performed by attaching handles to RNA. In such an experiment, which has not yet been done (however, see Note added), the H-RNA-H would be stretched by a stretching force $f_S > f_c$ so that RNA unfolds. By a feedback mechanism the force is quenched to $f_Q \neq 0$. We have simulated this situation for the H-P5GA-H construct with $L_H = 15 \text{ nm}$, $l_p^H = 30 \text{ nm}$ for each handle. We chose very stiff handles ($L_H < l_p^H$) so that the dynamics of RNA can be easily monitored. The end-to-end distance of the H-P5GA-H system as a function of t with $f_S = 90 \text{ pN}$ and $f_Q = 2 \text{ pN}$ shows a rapid decrease from $R_{sys} = 44 \text{ nm}$ to about $R_{sys} = 37 \text{ nm}$ in less than about $100 \mu\text{s}$ (Fig.11). The use of large values of f_S will not affect the results qualitatively. The value of R_{sys} fluctuates around 36 nm for a prolonged period and eventually R_{sys} attains its equilibrium value around 30 nm .

Upon decomposing R_{sys} into contributions from P5GA and the handle we find that the major changes in R_{sys} occur *when RNA undergoes the folding transition* (compare the top and middle panels in Fig.11). The time dependence of R_H , which monitors only the dynamics of the linker, shows that with $f_Q = 2 \text{ pN}$ after the initial relaxation R_H fluctuates around its equilibrium value (bottom panel in Fig.11).

From these simulations and others for different f_Q values we can make a few general comments that are relevant for experiments. (a) As long as $\lambda(= l_p^H/l_p^{RNA})$ is large enough the qualitative aspect of RNA folding can be obtained from the dynamics of R_{sys} alone. However, if $L_H/l_p^H \gg 1$ then large transverse fluctuations of the linker can interfere with the signal from RNA molecule. (b) To obtain quantitative results for the dynamics of RNA (i.e., R_M as a function of t) the dynamics of the handle upon force relaxation has to be described accurately. Upon $f_S \rightarrow f_Q$ quench the dynamics of the handle cannot be described using Langevin equation using the equilibrium force. Instead, the relaxation behavior must be determined by solving the Langevin equation for the WLC energy function [37] which is subject to $f_S \rightarrow f_Q$ quench.

DISCUSSIONS

Transition state movement and Hammond postulate for force: Hammond postulate [38, 39] is widely used to qualitatively predict the nature of transition state in the chemical reactions of organic molecules. In recent years a number of protein folding experiments have been interpreted using generalization of the Hammond postulate [40]. The Hammond postulate states that *if a transition state and an unstable intermediate, occur consecutively during a reaction process and have nearly the same energy, their interconversion will involve only a small reorganization of the molecular structure* [38]. In the context of RNA folding, the Hammond postulate suggests that *the position of the transition state along the reaction coordinate is shifted towards the destabilized state, either folded or unfolded, depending on the nature of perturbation*. The Hammond behavior is most vividly seen in the free energy profiles $F(R)$ (Fig.5-C) that pictorially describe mechanical unfolding of RNA hairpins. As f is increased the unfolded state is preferentially stabilized. From the Hammond postulate we would infer that the major TS should be more native-like as f increases. The force-dependent $F(R)$ as a function of R indeed confirms (Fig.5-C) that as f increases Δx_F^{TS} becomes closer to the native folded hairpin conformation.

RNA hairpins also denature upon heating. To ascertain the variation in the location of

the TS as temperature is changed we have calculated the free energy $F(Q)$ as a function of Q at several values of T at $f = 0$ (Fig.12-A). Although the location of the TS follows Hammond behavior there is *very little change* in the TS ensemble over the temperature range examined. Thus, the changes in the TS are very dramatic when unfolding is induced by force compared to thermal denaturation.

Hammond behavior can be quantified using the Leffler’s proportionality constant α_x which measures the energetic sensitivity of the transition state relative to the native states when the population shift is induced by a perturbation x [39, 41]. For mechanical unfolding ($x = f_S$)

$$\alpha_f = \frac{\partial \Delta F^\ddagger(R)/\partial f_S}{\partial \Delta F_{UF}(R)/\partial f_S} = \frac{\Delta x_F^{TS}}{\Delta x_{UF}}. \quad (17)$$

Using the free energy profile we computed α_f as a function of ΔF_{UF} or f (Fig.12-B). The shift in the transition state is, quantified by α_f in the range $0 \leq \alpha_f \leq 1$, and the shift rate (or self-interaction parameter, $p_f \equiv \partial \alpha_f / \partial \Delta F_{UF}$ [41]) has maximum in the force range $4 < f_S < 10$ pN. As ΔF_{UF} decreases (the UBA is stabilized with respect to the NBA) α_f decreases, which implies that the TS becomes increasingly native-like (Fig.12-B). The inset in Fig.12-B shows dramatically the changes in α_f with respect to f_S . The largest changes in α_f occurs as f_S approaches the T -dependent ($T = 290$ K) $f_c \approx 7$ pN. A similar plot of α_T as a function of T shows practically no change in α_T . From this analysis we conclude that the nature of the transition state ensemble is different in mechanical unfolding and thermal denaturation.

The transition state movement with force is very sensitive to the shape of the barrier in the vicinity of the transition state. The free energy profile near the barrier ($x \sim x_{ts}$) can be expanded as $F(x) \sim F(x_{ts}) - \frac{1}{2} F''(x_{ts})(x - x_{ts})^2 + \dots$. Upon application of the stretching force $F(x)$ is tilted by $-f_S \cdot x$. The new barrier position (x_{ts}^{NEW}) is at $x_{ts}^{NEW} \approx x_{ts} - f_S / F''(x_{ts})$. For a sharp transition barrier ($x_{ts} F''(x_{ts}) \gg f_S$), the force will not affect the position of the transition state ($x_{ts}^{NEW} \approx x_{ts}$). If the transition barrier is broadly distributed as in the unzipping pathway of RNA hairpins, the structure of transition state progressively changes as the magnitude of the force is varied. Typically, folding transition states are shallow and broad. As a result in biomolecular folding or unbinding, which involve formation or rupture of non-covalent interactions, we predict that the location of the TS depends on f_S and temperature. The assumption of a fixed TS used to interpret [5, 42, 43] experimental results is not valid. In addition, sequential [22] and/or parallel pathways to the stretched state transition [44, 45] are also possible. These observations suggest that a careful inspection of nonlinearity in the Arrhenius plot and α_f will be required to unravel barriers to unfolding.

Entropic barriers and long refolding times from fully stretched state: We have proposed that the long refolding time in P5GA upon force-quench from the initial stretched conformations is due to entropic barriers. The rate limiting step in the force-quench refolding of P5GA is the $t \rightarrow g^+$ transition in the nucleotides near the GAAA tetraloops. We analyze the simulation results by adopting a model proposed by Zwanzig [46]. In this Ising-like model each degree of freedom (in our case the dihedral angle) is presumed to exist in the “correct” state (native) and “incorrect” or non-native state. Suppose that the energy difference between the incorrect and correct states is ϵ and that there are N correct dihedral angles required for forming the hairpin loop. Let the free energy of loop stabilization be ϵ_{loop} . The energy, E_n , of a conformation with n -incorrect dihedral angles is $E_n = n\epsilon - \delta_{n0}\epsilon_{loop}$. If

we assume that the dihedral angle is a discrete variable with $1 + \nu$ states (ν is the number of incorrect states) then the partition function is

$$Z_N = \sum_{n=0}^N \binom{N}{n} \nu^n e^{-\beta(n\epsilon - \delta_{n0}\epsilon_{loop})} = e^{\beta\epsilon_{loop}} + (1 + \nu e^{-\beta\epsilon})^N - 1. \quad (18)$$

The thermal probability of realizing a conformation with n incorrect dihedral angles is

$$P_n(eq) = \frac{\binom{N}{n} \nu^n e^{-\beta(n\epsilon - \delta_{n0}\epsilon_{loop})}}{Z_N}. \quad (19)$$

The free energy profile, with n playing the role of a reaction coordinate for dihedral angle transitions, is $\Delta F(n) = n\epsilon - \delta_{n0}\epsilon_{loop} - k_B T \log \nu^n \binom{N}{n}$. For P5GA $N = 6$, $\epsilon \approx 2k_B T$, and $\epsilon_{loop} \approx 7.6k_B T$ ($= V_{STACK}^{B_8 B_9 B_{14} B_{13}} + V_{LJ}^{B_9 B_{14}} = 5.1k_B T + 2.5k_B T$). The free energy profile $\Delta F(n)$ (Fig.13) shows that the barrier depends only weakly on ν . Because the dihedral angle is a continuous variable, we use ν as an undetermined parameter. For $\nu = 13$ the free energy barrier (ΔF_F^\ddagger) is $\sim 2.7k_B T$, which leads to the observed increase ($\tau_F(f_Q = 0) = 15\tau_F(T)$) in the refolding time by factor of 15 ($= e^{\Delta F_F^\ddagger/k_B T}$).

The entropic barrier $\sim (5 - 6)k_B T$ is significantly larger than the free energy barrier ΔF_U^\ddagger in the absence of force. The barrier to the formation of conformations with $(ttttt)$ state in the loop region is large enough that they do not form by thermal fluctuations, and hence are irrelevant when refolding is initiated by temperature quench. However, such conformations are populated with near unit probability when fully stretched by mechanical force. When folding is initiated by force-quench from extended conformations (like conformation I in Fig.8-E), metastable conformations with incorrect dihedral angles in the loop regions are formed. These are characterized by plateaus in the dynamics of R (Fig.9-A). The crossing of the entropic barrier that places the loop dihedral angles in the native-like gauche state results in the slow refolding of P5GA hairpins. Once the loop is formed the zipping process quickly stabilizes the hairpin so that barrier crossing in reverse direction is unlikely to occur at low forces.

To further validate the proposed mechanism we performed simulations in which the value of the initial stretching force f_S is not large enough to fully extend the P5GA hairpin. In these simulations, the ensemble of initial structures is prepared so that they contain the preformed GAAA loop with only single bond before the loop region that is intact (see conformation II in Fig.8-E). The refolding kinetics follows a single exponential decay with a mean refolding time of $\sim 33 \mu s$, which is only 2-3 times longer than the refolding time of thermally denatured states. This value is much shorter than the refolding time from the fully stretched states ($> 191 \mu s$, see Fig.5-B). These simulations also show that τ_F is a function of both f_S and f_Q .

A byproduct of this analysis is that the appropriate reaction coordinate in force-quench refolding of RNA hairpins may be a local variable. In the formation of P5GA hairpin the local dihedral angles are the relevant reaction coordinates. The local dihedral coordinates, that describe the rate-limiting steps in the UBA \rightarrow NBA transition, are *hidden* in the global coordinates such as Q or R . Indeed, there is no correlation between the formation of native dihedral angles in the GAAA tetraloop and global order parameters. We infer that to describe folding, especially of RNA, multiple reaction coordinates that describe the

hierarchical assembly are required.

Difficulties in extracting energy landscape parameters from single molecule force spectroscopy: Several studies [31, 42] have pointed out the inherent ambiguities in quantitatively characterizing the energy landscape from measurable quantities in dynamic force spectroscopy. From the plots $[f^*, \log r_f]$ one cannot unambiguously obtain the location of the transition state(s) or even the number of free energy barriers [42]. The significant curvatures in the $[f^*, \log r_f]$ plots are usually interpreted in terms of multiple transition states [22, 42]. In our example, the P5GA hairpin unfolds upon application of force by *crossing a single free energy barrier*. Explicit equilibrium $F(R)$ profiles (Fig.5-C) and experiments [5] that have monitored hopping dynamics in P5ab hairpin show that there is only one free energy barrier in these simple structures. Nevertheless, $[f^*, \log r_f]$ plot is highly nonlinear (Fig.4-B). In the hairpin case we have shown that the non-linearity is due to the dramatic changes in Δx_U^{TS} as r_f is varied. The standard assumption that Δx_U^{TS} is a constant breaks down, and is likely to be an even more of a severe approximation for RNA with tertiary structures.

To further illustrate the importance of transition state movements we consider a trivial one dimensional potential

$$E(x) = -\epsilon \exp(-\xi x). \tag{20}$$

In this barrierless potential a particle is “unbound” if $|E(x_{ts})/k_B T| < 1$ where x_{ts} is the TS location. Upon application of a constant f_S the potential becomes

$$E(x) = -\epsilon \exp(-\xi x) - f_S x. \tag{21}$$

The location of the transition state in the force range $0 < f_S < \xi \epsilon$ is

$$x_U^{TS} = -\frac{1}{\xi} \log f_S / \xi \epsilon. \tag{22}$$

If $f_S > \xi \epsilon$ then $x_U^{TS}(f) = 0$ and the particle is always unbound (Fig.14-A). The changes in x_U^{TS} can lead to significant deviations from the Bell equation even in constant f_S -experiments. The distribution of unbinding forces upon deforming the potential at constant loading rate ($f_S(t) = r_f t$) can be analytically obtained (see Eq.(8) in [47]). The $[f^*, \log r_f]$ plot from these calculations show non-linearities (Fig.14-B) that are similar to what is found for P5GA (Fig.4-B). In both instances the reason for curvature is entirely due to r_f -dependent changes in the TS location.

CONCLUSIONS

We have systematically investigated forced-unfolding and force-quench refolding of RNA hairpins. Using a general minimal model for RNA we have obtained a number of new results that give a molecular picture of unfolding and refolding of RNA hairpins triggered by force. Although they were obtained specifically for P5GA we expect the conclusions to be valid for other RNA sequences as well. The specific predictions, that are amenable to experimental test, of our study are listed below.

- 1) Besides probing the energy landscape using f as a “denaturant” one of the goals of single molecule studies is to extract intrinsic parameters like folding (k_F^o) and unfolding rates

(k_U^o) and the nature of the transition state in the absence of force. However, extraction of the kinetic parameters from dynamic force spectroscopy is fraught with difficulties because several models can produce similar $[f^*, \log r_f]$ profiles. Here we have shown, for a system *that has only a single barrier to unfolding*, that Δx_U^{TS} depends dramatically on f_S and r_f . The movements in the TS is intrinsic to properties of RNA hairpins and are clearly reflected in the free energy profiles. Combining the present results and our previous study [14] we surmise that Δx_U^{TS} is dependent on T and f . Thus, extrapolations to zero force to obtain reliable estimates of unfolding rates requires not only accounting for free energy barriers [31] but also on the dependence of Δx_U^{TS} on T and f . Only by performing multiple experiments (or simulations) over a range of f_S and T can the free energy landscape be fully characterized.

- 2) An important prediction of our work is that refolding times upon force-quench $\tau_F(f_Q)$ from stretched states are much greater than those obtained by temperature quench. More generally, $\tau_F(f_Q)$ depends, sensitively on the initial value of the stretching force. The microscopic origin of the long force-quench refolding times in P5GA has been traced to the time needed for the trans→gauche transition in the GAAA tetraloop region. From this observation we predict that refolding time $\tau_F(f_Q)$ should be very long compared to thermal refolding times for P5ab which also has the GAAA tetraloop. Because the refolding times for RNA hairpins are determined by the local structural features in the initial stretched states we suggest that, at a fixed temperature, $\tau_F(f_Q)$ might *depend upon only weakly* on the helix length or the precise sequence (percentage of GC for example).
- 3) Dissecting the folding mechanism of RNA is difficult because of an interplay of a number of factors [48]. We predict that refolding mechanisms (pathways and the nature of the transition state ensemble) by temperature (or by increasing cation concentration) and force quench have to be drastically different. In the former, the transition to the low entropic NBA proceeds from a high entropy relatively compact state whereas in the latter it occurs from a low entropy stretched state [49]. The predicted dramatic differences in the folding mechanisms can be established by probing force-quench refolding at fixed T and counterion concentration.

The present model has a number of limitations. The use of Go model for force-unfolding may not be a serious approximation because unfolding pathway are largely determined by the native topology [50]. However, the neglect of non-native interactions will have dramatic effect on refolding. At a minimum, the roughness ($\delta\epsilon$) of the energy landscape is underestimated by the Go model. The importance of $\delta\epsilon$ can be assessed by doing forced-unfolding experiments over a range of temperature [47, 51]. Finally, the electrostatic interactions in RNA have been modeled in the simplest manner that is only appropriate for monovalent cation [52]. To address the effect of counterion (Mg^{2+} or polyanions) explicit modeling of the cations will be required.

APPENDIX I

In this appendix we describe the procedure for determining the persistence length of the linkers used in our simulations. For the linker molecules, whose energy function is given

by Eq.(9), we calculated the persistence length by fitting the worm-like chain end-to-end (R) distribution function ($P_{WLC}(R)$) [53] to the simulated $P(R)$. We adopted Monte Carlo simulation with Pivot algorithm [54] to generate a large number of equilibrium conformations of the linker molecule. Given $k_B(= 20 \text{ kcal}/(\text{mol} \cdot \text{\AA}^2))$, $k_A(= 20 \text{ kcal}/\text{mol}$ or $80 \text{ kcal}/\text{mol}$), and varying N the number of monomers in the WLC linker, we obtained the unknown parameters, namely, the contour length (L) and the persistence length (l_p) by fitting $P(R)$ to

$$P_{WLC}(R) = \frac{4\pi C(R/L)^2}{L[1 - (R/L)^2]^{9/2}} \exp\left[-\frac{3t}{4(1 - (R/L)^2)}\right]. \quad (23)$$

where $t \equiv L/l_p$. The normalization constant $C = 1/[\pi^{3/2}e^{-\alpha}\alpha^{-3/2}(1 + 3\alpha^{-1} + 15/4\alpha^{-2})]$ with $\alpha = 3t/4$, satisfies $\int_0^L dR P_{WLC}(R) = 1$. The dependence of the persistence length of the linkers, as a function of N is displayed in Fig.15. The quality of the fit improves as N becomes larger (data not shown). We also computed the persistence length and the contour length of P5GA at $T > T_m$ using the same fitting procedure, which gives $l_p^{RNA} \approx 1.5 \text{ nm}$ and $L = 12.5 \text{ nm}$ (Fig.15-inset on the bottom). In our simulations $\lambda = l_p^H/l_p^{RNA}$ ranges from $10 < \lambda < 70$. The experimental value of $\lambda \approx 50$ [5]

Acknowledgments: This work was supported in part by a grant from the National Science Foundation (CHE 05-14056).

Note added: While the present paper was under review refolding upon force-quench of TAR RNA was reported [55]. In accord with the present and our previous studies [14], force-quench refolding times are relatively long. The distributions of refolding times similar to the curves in Fig.6, as a function of f_Q were not reported in [55]. Thus, it is unclear if there is a lag phase in the force quench refolding of TAR RNA.

-
- [1] Doudna, J. and T, Cech. 2002. The chemical repertoire of natural ribozymes. *Nature* 418:222–228.
- [2] Onoa, B. and I. Tinoco, Jr. 2004. RNA folding and unfolding. *Curr. Opin. Struct. Biol.* 14:374–379.
- [3] Tinoco Jr., I. 2004. Force as a useful variable in reactions: Unfolding RNA. *Ann. Rev. Biophys. Biomol. Struct.* 33:363–385.
- [4] Bustamante, C., Y. R. Chemla, N. R. Forde, and D. Izhaky. 2004. Mechanical processes in biochemistry. *Ann. Rev. Biochem.* 73:705–748.
- [5] Liphardt, J., B. Onoa, S. B. Smith, I. Tinoco, Jr., and C. Bustamante. 2001. Reversible unfolding of single RNA molecules by mechanical force. *Science* 292:733–737.
- [6] Onoa, B., S. Dumont, J. Liphardt, S. B. Smith, I. Tinoco, Jr., and C. Bustamante. 2003. Identifying Kinetic Barriers to Mechanical Unfolding of the *T. thermophila* Ribozyme. *Science* 299:1892–1895.
- [7] Rief, M., M. Gautel, F. Oesterhelt, J. M. Fernandez, and H. E. Gaub. 1997. Reversible Unfolding of Individual Titin Immunoglobulin Domains by AFM. *Science* 276:1109–1111.
- [8] Fernandez, J. and H. Li. 2004. Force-Clamp Spectroscopy Monitors the Folding Trajectory of a Single Protein. *Science* 303:1674–1678.
- [9] Gerland, U., R. Bundschuh, and T. Hwa. 2001. Force-Induced Denaturation of RNA. *Biophys. J.* 81:1324–1332.
- [10] Mueller, M., F. Krzakala, and M. Mezard. 2002. The secondary structure of RNA under tension. *Eur. Phys. J. E* 9:67–77.
- [11] Gerland, U., R. Bundschuh, and T. Hwa. 2003. Mechanically Probing the Folding Pathway of Single RNA Molecules. *Biophys. J.* 84:2831–2840.
- [12] Cocco, S., J. Marko, and R. Monasson. 2003. Slow nucleic acid unzipping kinetics from sequence-defined barriers. *Eur. Phys. J. E* 10:153–161.
- [13] Manosas, M. and F. Ritort. 2005. Thermodynamic and Kinetic Aspects of RNA pulling experiments. *Biophys. J.* 88:3224–3242.
- [14] Hyeon, C. and D. Thirumalai. 2005. Mechanical unfolding of RNA hairpins. *Proc. Natl. Acad.*

- Sci.* 102:6789–6794.
- [15] Bell, G. I. 1978. Models for the specific adhesion of cells to cells. *Science* 200:618–627.
- [16] Cate, J. H., A. R. Gooding, E. Podell, K. Zhou, B. L. Golden, C. E. Kundrot, T. R. Cech, and J. A. Doudna. 1996. Crystal Structure of a Group I Ribozyme Domain: Principles of RNA Packing. *Science* 273:1678–1685.
- [17] Rudisser, S. and I. Tinoco, Jr. 2000. Solution Structure of Cobalt(III)Hexammine Complexed to the GAAA Tetraloop, and Metal-ion Binding to GA Mismatches. *J. Mol. Biol.* 295:1211–1223.
- [18] Walter, A. E., D. H. Turner, J. Kim, M. H. Lyttle, P. Muller, D. H. Mathews, and M. Zuker. 1994. Coaxial stacking of helices enhances binding of oligoribonucleotides and improves predictions of RNA folding. *Proc. Natl. Acad. Sci. USA* 91:9218–9222.
- [19] Mathews, D., J. Sabina, M. Zuker, and D. Turner. 1999. Expanded Sequence Dependence of Thermodynamic Parameters Improves Prediction of RNA Secondary Structure. *J. Mol. Biol.* 288:911–940.
- [20] Dima, R. I., C. Hyeon, and D. Thirumalai. 2005. Extracting stacking interaction parameters for RNA from the data set of native structures. *J. Mol. Biol.* 347:53–69.
- [21] Misra, V. and D. Draper. 2001. A thermodynamic framework for Mg^{2+} binding to RNA. *Proc. Natl. Acad. Sci.* 98:12456–12461.
- [22] Merkel, R., P. Nassoy, A. Leung, K. Ritchie, and E. Evans. 1999. Energy landscapes of receptor-ligand bonds explored with dynamic force spectroscopy. *Nature* 397:50–53.
- [23] Lee, N. and D. Thirumalai. 2004. Pulling-speed-dependent force-extension profiles for semi-flexible chains. *Biophys. J.* 86:2641–2649.
- [24] Veitshans, T., D. Klimov, and D. Thirumalai. 1996. Protein folding kinetics: timescales, pathways and energy landscapes in terms of sequence-dependent properties. *Folding Des.* 2:1–22.
- [25] Ermack, D. and J. McCammon. 1978. Brownian dynamics with hydrodynamic interactions. *J. Chem. Phys.* 69:1352–1369.
- [26] Klimov, D., M. Betancourt, and D. Thirumalai. 1998. Virtual atom representation of hydrogen bonds in minimal off-lattice models of alpha helices: effect on stability, cooperativity and kinetics. *Folding Des.* 3:481–498.

- [27] Ferrenberg, A. M. and R. H. Swendsen. 1988. New monte carlo technique for studying phase transitions. *Phys. Rev. Lett.* 61:2635–2638.
- [28] Kumar, S., D. Bouzida, R. H. Swendsen, P. A. Kollman, and J. M. Rosenberg. 1992. The weighted histogram analysis method for free-energy calculation on biomolecules. I. The method. *J. Comp. Chem.* 13:1011–1021.
- [29] Nymeyer, H., A. E. Garcia, and J. N. Onuchic. 1998. Folding funnels and frustration in off-lattice minimalist protein landscapes. *Proc. Natl. Acad. Sci.* 95:5921–5928.
- [30] Reif, M., H. Gautel, F. Oesterhelt, J. M. Fernandez, and H. Gaub. 1997. Reversible unfolding of individual titin immunoglobulin domains by AFM . *Science* 276:1109–1112.
- [31] Hummer, G. and A. Szabo. 2003. Kinetics from Nonequilibrium Single-Molecule Pulling Experiments. *Biophys. J.* 85:5–15.
- [32] Fernandez, J. M., H. Li, and J. Brujic. 2004. Response to Comment on "Force-Clamp Spectroscopy Monitors the Folding Trajectory of a Single Protein". *Science* 306:411c.
- [33] Khorasanizadeh, S., I. D. Peters, T. R. Butt, and , H. Roder. 1993. Folding and stability of a tryptophan-containing mutant of ubiquitin. *Biochemistry* 32:7054–7063.
- [34] Krantz, B. A., L. Mayne, J. Rumbley, S. W. Englander, and T. R. Sosnick. 2002. Fast and slow intermediate accumulation and the initial barrier mechanism in protein folding. *J. Mol. Biol.* 324:359–371.
- [35] Sosnick, T. R. 2004. Comment on "Force-Clamp Spectroscopy Monitors the Folding Trajectory of a Single Protein". *Science* 306:411b.
- [36] Best, R. B. and G. Hummer. 2005. Comment on "Force-Clamp Spectroscopy Monitors the Folding Trajectories of a Single Protein". *Science* 308:498b.
- [37] Bohbot-Raviv, Y., W. Z. Zhao, M. Feingold, C. H. Wiggins, and R. Granek. 2004. Relaxation Dynamics of Semiflexible Polymers. *Phys. Rev. Lett.* 92:098101.
- [38] Hammond, G. S. 1953. A correlation of reaction rates. *J. Am. Chem. Soc.* 77:334–338.
- [39] Leffler, J. E. 1953. Parameters for the description of transition states. *Science* 117:340–341.
- [40] Fersht, A. R. 1999. *Structure and mechanism in protein science*. Freeman.
- [41] Sánchez, I. E. and T. Kiefhaber. 2003. Hammond behavior versus ground state effects in protein folding: Evidence for narrow free energy barriers and residual structure in unfolded States. *J. Mol. Biol.* 327:867–884.

- [42] Derenyi, I., D. Bartolo, and A. Ajdari. 2004. Effects of intermediate bound states in dynamic force spectroscopy. *Biophys. J.* 86:1263–1269.
- [43] Evans, E. and K. Ritchie. 1997. Dynamic Strength of Molecular Adhesion Bonds. *Biophys. J.* 72:1541–1555.
- [44] Nevo, R., C. Stroh, F. Kienberger, D. Kaftan, V. Brumfeld, M. Elbaum, Z. Reich, and P. Hinterdorfer. 2003. A molecular switch between alternative conformational states in the complex of Ran and importin β 1. *Nature. Struct. Biol.* 10:553–557.
- [45] Barsegov, V. and D. Thirumalai. 2005. Dynamics of unbinding of cell adhesion molecules: Transition from catch to slip bonds. *Proc. Natl. Acad. Sci.* 102:1835–1839.
- [46] Zwanzig, R. 1995. Simple model of protein folding kinetics. *Proc. Natl. Acad. Sci.* 92:9801–9804.
- [47] Hyeon, C. and D. Thirumalai. 2003. Can energy landscape roughness of proteins and RNA be measured by using mechanical unfolding experiments? *Proc. Natl. Acad. Sci.* 100:10249–10253.
- [48] Thirumalai, D. and C. Hyeon. 2005. RNA and Protein folding: Common Themes and Variations. *Biochemistry* 44:4957–4970.
- [49] Li, M. S., C. K. Hu, D. K. Klimov, and D. Thirumalai. Multiple stepwise refolding of immunoglobulin I27 upon force quench depends on initial conditions. *Proc. Natl. Acad. Sci.* in press.
- [50] Klimov, D. and D. Thirumalai. 2000. Native topology determines force-induced unfolding pathways in globular proteins. *Proc. Natl. Acad. Sci. USA* 97:7254–7259.
- [51] Nevo, R., V. Brumfeld, R. Kapon, P. Hinterdorfer, and Z. Reich. 2005. Direct measurement of protein energy landscape roughness. *EMBO reports* 6:482.
- [52] Lee, N. K. and D. Thirumalai. 1999. Stretching DNA: Effect of electrostatic interactions. *Europhys. J. B.* 12:599–605.
- [53] Thirumalai, D. and B. Y. Ha. 1998. Statistical Mechanics of Semiflexible Chains: A Mean Field Variational Approach. In *Theoretical and Mathematical Models in Polymer Research*. A. Grosberg, editor. Academic Press, San Diego. 1–35.
- [54] Bishop, M., J. H. R. Clarke, A. Rey, and J. J. Freire. 1991. Investigation of the end-to-end vector distribution function for linear polymer in different regimes. *J. Chem. Phys.* 95:4589–4592.

- [55] Li, P. T. X., D. Collin, S. B. Smith, C. Bustamante, and I. Tinoco Jr. Probing the Mechanical Folding Kinetics of TAR RNA by Hopping, Force-Jump, and Force-Ramp Methods *Biophys. J.* 90:250–260.

FIGURE CAPTION

Figure 1 : Coarse-grained representation of a RNA using three (phosphate (P), sugar (S) and base (B)) interaction sites per nucleotide. On the left we present the secondary structure of the 22-nt P5GA hairpin in which the bonds formed between base pairs are labeled from 1 to 9. The PDB structure [17] and the lowest energy structure obtained with the coarse-grained model are shown on the right.

Figure 2 : **A.** Schematic illustration of laser optical tweezer (LOT) setup for RNA stretching. Single RNA molecule is held between two polystyrene beads via molecular handles with one of the polystyrene beads being optically trapped in the laser light. The location of the other bead is changed by manipulating it by a micropipette. The extension of the molecule through the molecular handles induces the deviation in the position of the polystyrene bead held in the force-measuring optical trap. **B.** Both LOT and AFM can be conceptualized as schematically shown. The RNA molecule is sandwiched between the linkers and one end of the linker is pulled. The spring constant of the harmonic trap in LOT (or the cantilever in AFM experiments) is given by k and v is the pulling speed.

Figure 3 : Unfolding pathways upon temperature and force jump. **A.** The time dependence of rupture of the bonds is monitored when the temperature is raised from $T(= 100 K) < T_m(\approx 341 K)$ to $T(= 346 K) > T_m$. The set of nine bonds are disrupted stochastically. **B.** In forced unfolding bonds rip from the ends to the loop regions in an apparent staircase pattern. For both **A** and **B** the scale indicating the probability of a given bond being intact is given below. **C.** Free energy $F(Q)$ as a function of Q . The stable hairpin with $Q \approx 1$ at $T = 100 K$ becomes unstable upon rapid temperature jump to $T = 346 K$ (blue *). Subsequent to the T-jump the hairpin relaxes to the new equilibrium state by crossing a small free energy barrier ($\approx 0.5 kcal/mol$) with $Q \approx 0.2$. The inset shows the equilibrium free energy profile at $T = 346 K$ and $f = 0$. **D.** Deformation of the free energy profile upon application of force. The R dependent free energy $F(R) = F(R; f_S = 0) - f_S \cdot R$ favors the stretched state at $R = 12 nm$ when $f = 42 pN$ (see inset). The activation barrier separating the UBA and NBA is around $(1-2)kcal/mol$.

Figure 4 : Constant loading rate force unfolding. **A.** The unfolding force distributions at different pulling speeds with hard ($k = 70 pN/nm$, up) and soft springs ($k = 0.7 pN/nm$, down). For the hard spring, the pulling speeds from right to left are $v = 8.6 \times 10^4, 8.6 \times 10^3, 8.6 \times 10^2 \mu m/s$. For the soft spring, the pulling speeds are $v = 8.6 \times 10^4, 1.7 \times 10^4, 8.6 \times 10^3, 8.6 \times 10^2, 8.6 \times 10^1 \mu m/s$ from right to left force peaks. The peak in the distributions which are fit to a Gaussian is the most probable force f^* . **B.** The dependence of f^* as a function of the loading rates, r_f . The results from the hard spring and soft spring are combined using the loading rate as the relevant variable. The inset illustrates the potential difficulties in extrapolating from simulations at large r_f to small values of r_f .

Figure 5 : Kinetics of forced-unfolding and force-quench refolding: **A.** Plot of force-induced unfolding times (τ_U) as a function of the stretching force. Over a narrow range of force τ_U decreases exponentially as f increases. **B.** Refolding time τ_F as a function of f_Q . The initial value of the stretching force is $90 pN$. By fitting τ_F using $\tau_F(f_Q) = \tau_F^o \exp(f_Q \Delta x_F^{TS}/k_B T)$, in the range of $0.5 pN < f_Q < 4 pN$, we obtain $\Delta x_F^{TS} \approx 1 nm$ and $\tau_F^o \approx 290 \mu s$. **C.** Changes in the equilibrium free energy profiles at $T = 290 K$ $F(R)$ as a function of the variable R . We show $F(R)$ at various f_S values. For emphasis, the free energies at $f_S = 0$ and at the transition midpoint $f_S = 7.5 pN$ (dashed line) are drawn in

thick lines.

Figure 6 : Time dependence of the probability that RNA is unfolded upon force quench. In these simulation $T = 290 K$, and the initial stretching force $f_S = 90 pN$ and f_Q (values are given in each panel), the quench force, is varied. The simulation results are fit using Eq.(14) which is obtained using the kinetic scheme $S \xrightarrow{\tau_1} I \xrightarrow{\tau_2} F$. Here, I represents conformations with in certain fraction of incorrect dihedral angles. The time constants (τ_1, τ_2) , in μs , at each force are: (81.2, 101.3) at $f_Q = 0 pN$, (159.5, 160.8) at $f_Q = 0.5 pN$, (180.0, 174.8) at $f_Q = 1 pN$, (237.6, 240.5) at $f_Q = 2 pN$, (326.8, 335.6) at $f_Q = 3 pN$, and (347.7, 329.7) at $f_Q = 4 pN$.

Figure 7 : **A.** The equilibrium distribution of the end-to-end distance at extremely high temperature ($T = 1500 K$). Even at this elevated temperature the fully stretched conformations of $R = 13.5 nm$ (arrow) is not found in the ensemble of thermally denatured conformations. **B.** Refolding is initiated by a force quench from the initial value $f_S = 90 pN$ to $f_Q = 4 pN$. The five time traces show great variations in the relaxation to the hairpin conformation. However, in all trajectories R decreases in at least three distinct stages that are explicitly labeled for the trajectory in green.

Figure 8 : **A.** The dihedral angles of the P5GA hairpin in the native state. All the dihedral angles are in the trans form except 19-th position of dihedral angle which is in the gauche(+) conformation (indicated by orange circle). **B.** The dihedral angle potentials for trans (top) and gauche(+) form (bottom) are plotted using Eq.(3). The red lines show the potentials in the loop region. **C, D.** The average deviation of the i -th dihedral angle relative to the native state is computed using the 100 different structures generated by high temperature ($T = 500 K$) (**C**) and by force ($R = 13.5 nm$) (**D**). To express the deviations of the dihedral angles from their native state values we used $1 - \cos(\phi_i - \phi_i^o)$ for i -th dihedral angle ϕ_i where ϕ_i^o is the i -th dihedral angle of the native state. **E.** A snapshot of fully stretched hairpin (I). Note the transition in 19-th dihedral angle undergoes $g^+ \rightarrow t$ transition when hairpin is stretched. An example of a partially stretched conformation (II) with the GAAA tetraloop and bond 9 intact. Refolding times starting from these conformations are expected to be shorter than those that start from fully stretched states.

Figure 9 : **A.** A sample refolding trajectory starting from the stretched state. The hairpin was initially unfolded to a fully stretched state and f_Q was set to zero at $t \approx 20 \mu s$. End-to-end distance monitored as a function of time shows that refolding occurs in steps. **B.** The deviation of dihedral angles from their values in native state as a function of time. The large deviation of the dihedral angles in loop region can be seen in the red strip. Note that this strip disappears around $t \approx 300 \mu s$, which coincides with the formation of bonds shown in **C**. f_B is the fraction of bonds with pink color indicating that the bond is fully formed.

Figure 10 : The force extension curves (FECs) of RNA hairpin at constant pulling speed and varying linker lengths and flexibilities. The pulling speed, $v = 0.86 \times 10^2 \mu m/s$. The spring constant, $k = 0.7 pN/nm$. FECs from different linker lengths are plotted in black (10 nm), red (20 nm), green (30 nm), blue (40 nm), and orange (50 nm). **A.** This panel shows the experimentally relevant plots, namely, FECs for H-RNA-H construct. The signature for the hairpin opening transition region is ambiguous at large L_H values. **B.** FECs only for P5GA corresponding to different L_H values. The FEC for the linker is subtracted from (A). The gradual increase of rupture force is observed as L increases. The value of k_A (Eq.(9)) of linker polymer used in (A) and (B) is $80 kcal/(mol \cdot \text{\AA})$. **C.** Comparison between FECs with $L_H (= 40 nm)$ fixed but at different k_A values. Red curve is the average of 7 individual

FECs that are shown in orange ($80 \text{ kcal}/(\text{mol} \cdot \text{\AA})$). Black curve is the average of 9 individual FECs in grey ($20 \text{ kcal}/(\text{mol} \cdot \text{\AA})$). Less stiff linker leads to slightly larger unfolding force. It should be stressed that for both values of k_A the λ ratio is large.

Figure 11 : Refolding trajectory of RNA that is attached to the handles. Linkers with $L_H = 15 \text{ nm}$ and $l_p^H = 30 \text{ nm}$ are attached to both side of RNA hairpin. The initial force (90 pN) stretched P5GA to 14 nm . The value of $f_Q = 2 \text{ pN}$. The top panel shows the dynamics of the end-to-end distance, R_{sys} , of H-P5GA-H. The middle panel corresponds to the end-to-end distance of P5GA. The end-to-end distances, R_H , of the 3' and 5'-side handles fluctuates around its equilibrium value of 14 nm after the initial rapid relaxation. The right panels show the decomposition of R_H into the longitudinal and the transverse components. The value of $R_H^{\parallel} \approx 13 \text{ nm}$ agrees well with the equilibrium value obtained by solving $f_Q = k_B T / l_p^H \left(R_H^{\parallel} / L_H + 1/4 \left(1 - \frac{R_H^{\parallel}}{L_H} \right)^2 - 1/4 \right)$ with $f_Q = 2 \text{ pN}$.

Figure 12 : **A.** Free energy profiles of Q at different temperatures. Note that the positions of the transition states over the temperature variation almost remain constant. **B.** The movement of transition state measured in terms of the Leffler parameter (Eq.(17)). The structural nature of transition state is monitored by the free energy difference between NBA and UBA when f is a external variable. The inset shows the variation of α with respect to force. The value of $T = 290 \text{ K}$.

Figure 13 : The free energy as a function of the number of incorrect dihedral angles calculated using the Zwanzig model (see text for details). As the number of distinct values (ν) that the dihedral angle can take increases the entropic barrier increases. For P5GA $\nu = 13$ provides the best fit of the model to simulations (see text).

Figure 14: **A.** Sketch of the one-dimensional potential $E(x)$ as a function of x for several values of f_S . The transition state location is obtained using $E'(x_{ts}) = 0$. The boundary separating bound and unbound states is given by $|E(x_{ts})/k_B T| = 1$. **B.** Dependence of the most probable “unbinding” force f^* as a function of r_f . The $[f^*, \log r_f]$ plot for the artificial potential is similar to that shown in Fig.4-B.

Figure 15 : Persistence length l_p as a function of contour length L for linkers at 290 K . The number of monomers N (Eq.(9)) is also shown. The values of l_p and L are obtained by fitting the end-to-end distance distribution function $P(R)$ generated by simulations to the theoretical expression based on a mean field model (Eq.(23)). An example of such a fit for a linker with $N = 50$ using two different values of k_A (see Eq.(9)) is shown in the inset on the top. For large N , l_p converges to a constant value. The fit of simulated $P(R)$ for P5GA computed at $T(= 500 \text{ K}) > T_m$ is shown in the inset on the bottom. From the WLC fit we obtain $l_p \approx 1.5 \text{ nm}$ and $L = 12.5 \text{ nm}$ for P5GA.

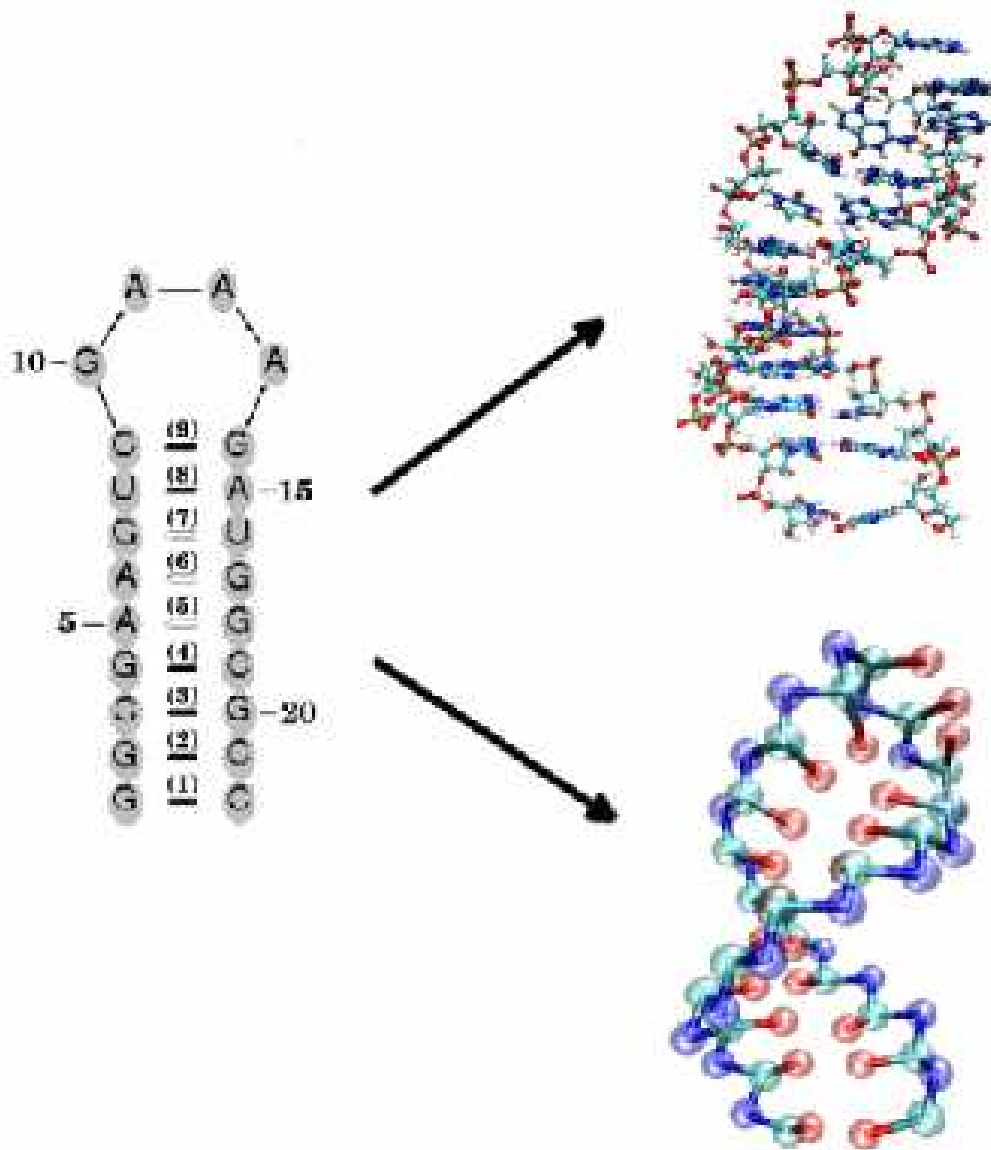


FIG. 1:

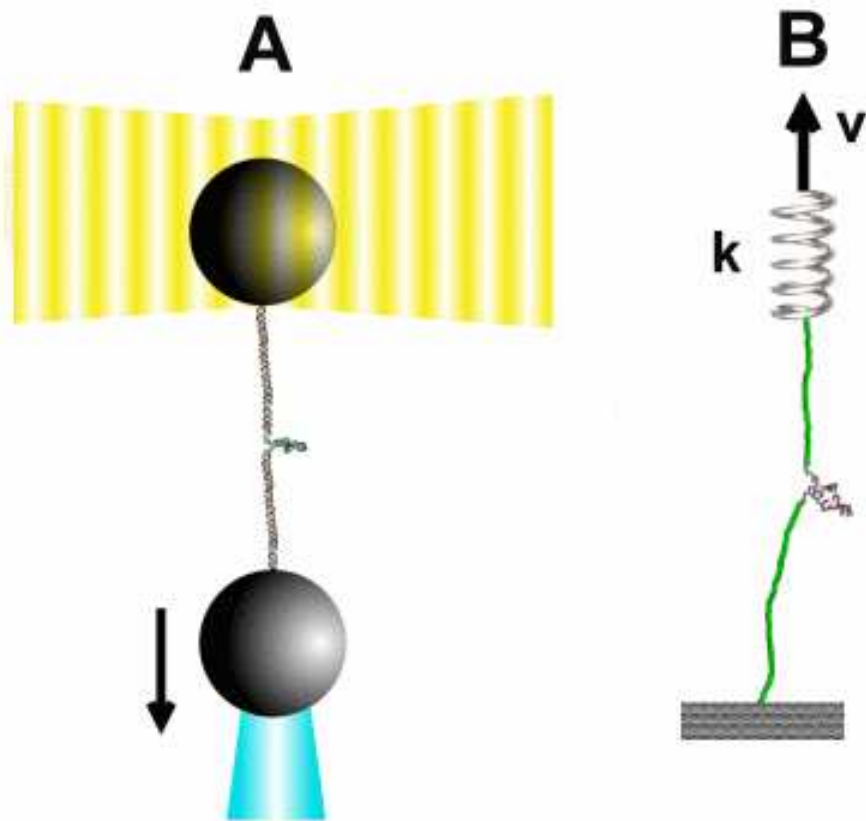


FIG. 2:

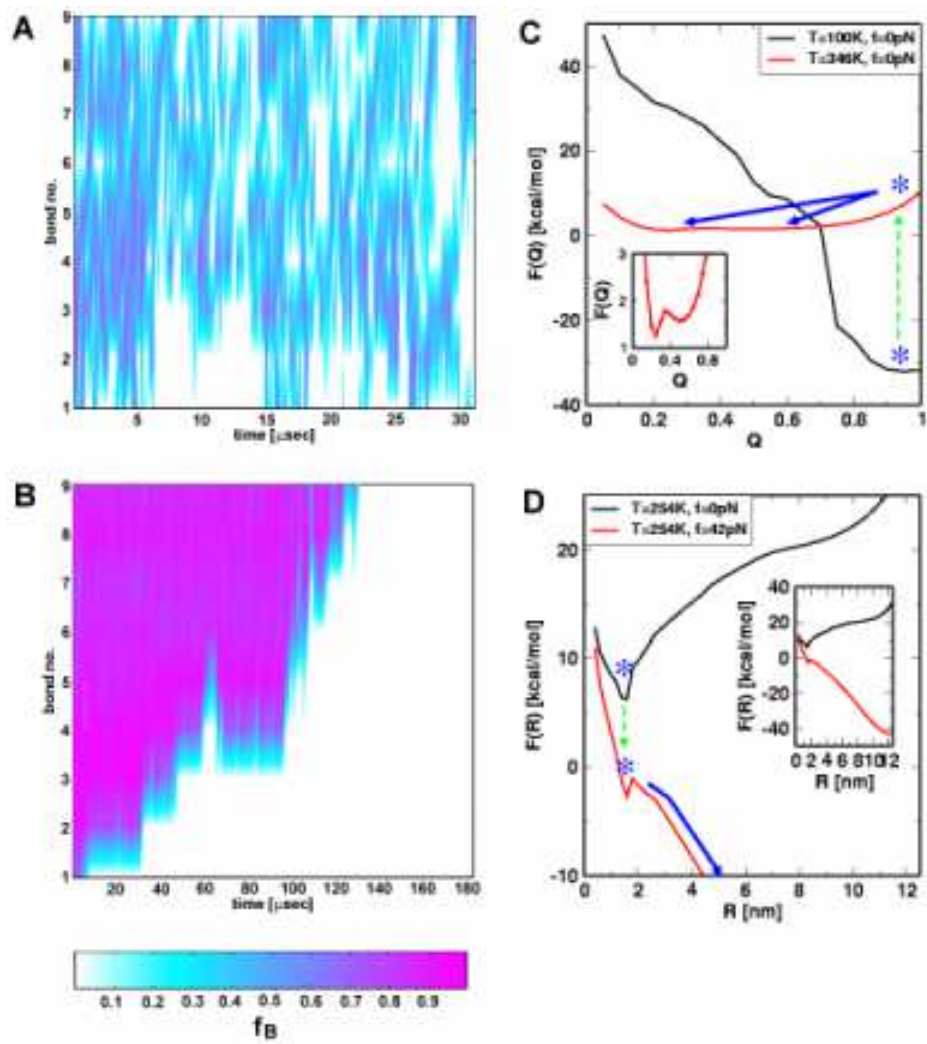


FIG. 3:

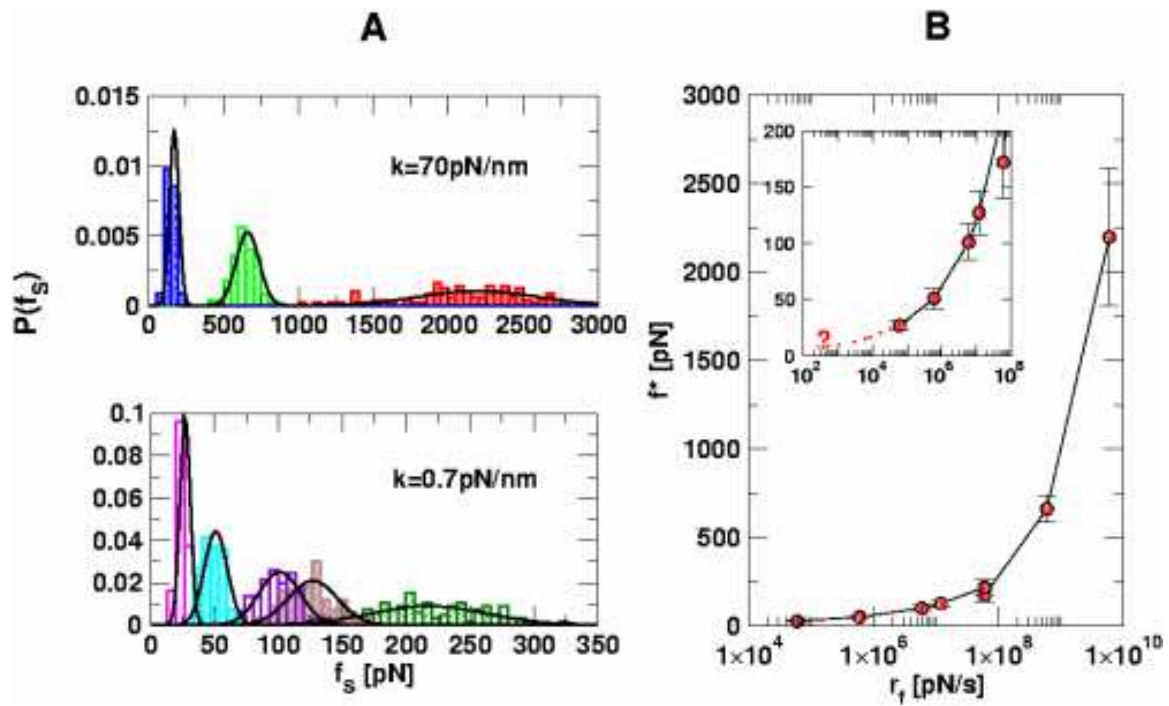


FIG. 4:

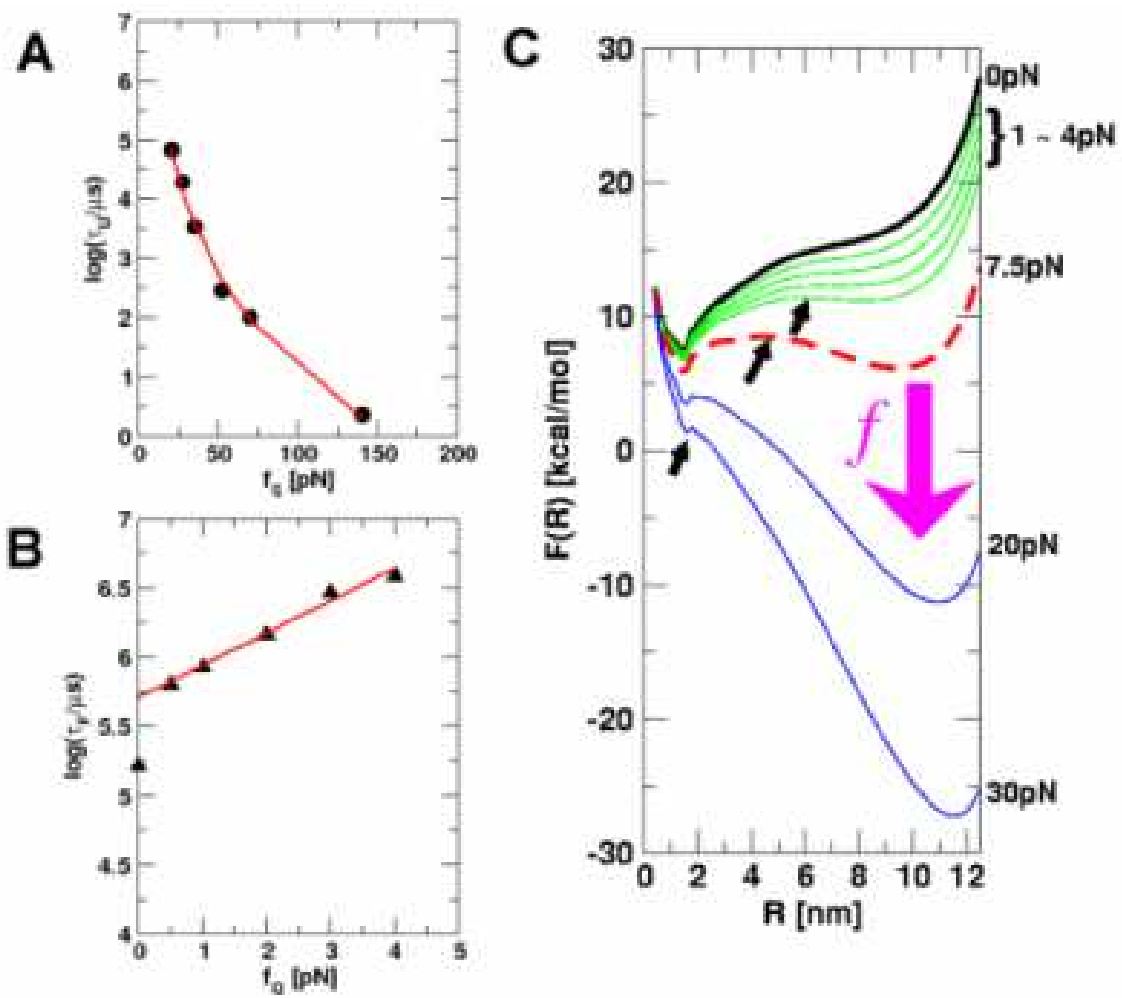


FIG. 5:

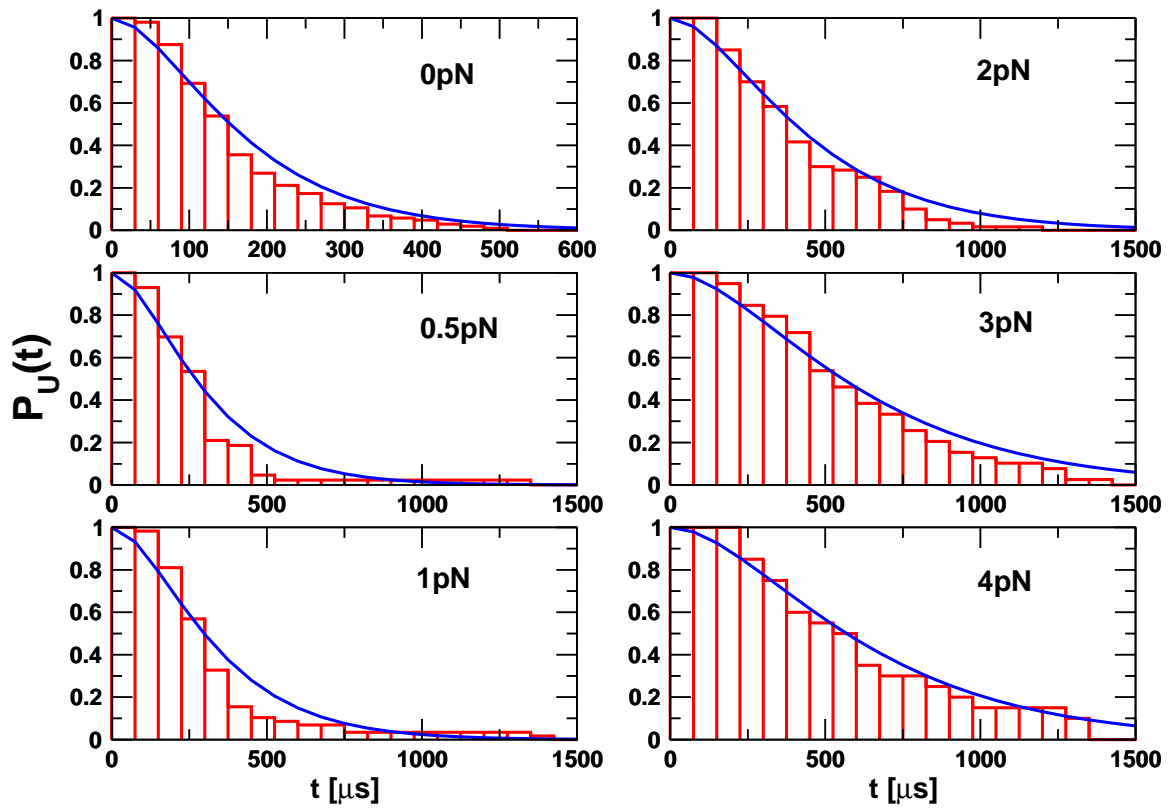


FIG. 6:

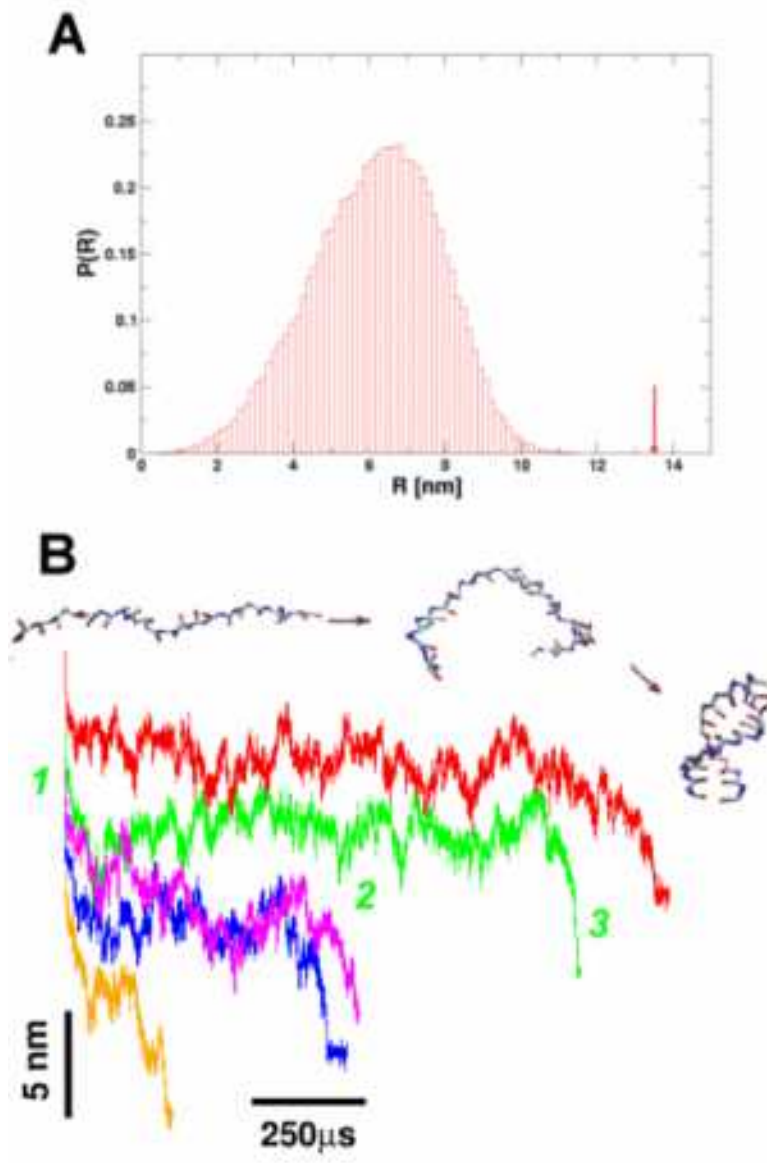


FIG. 7:

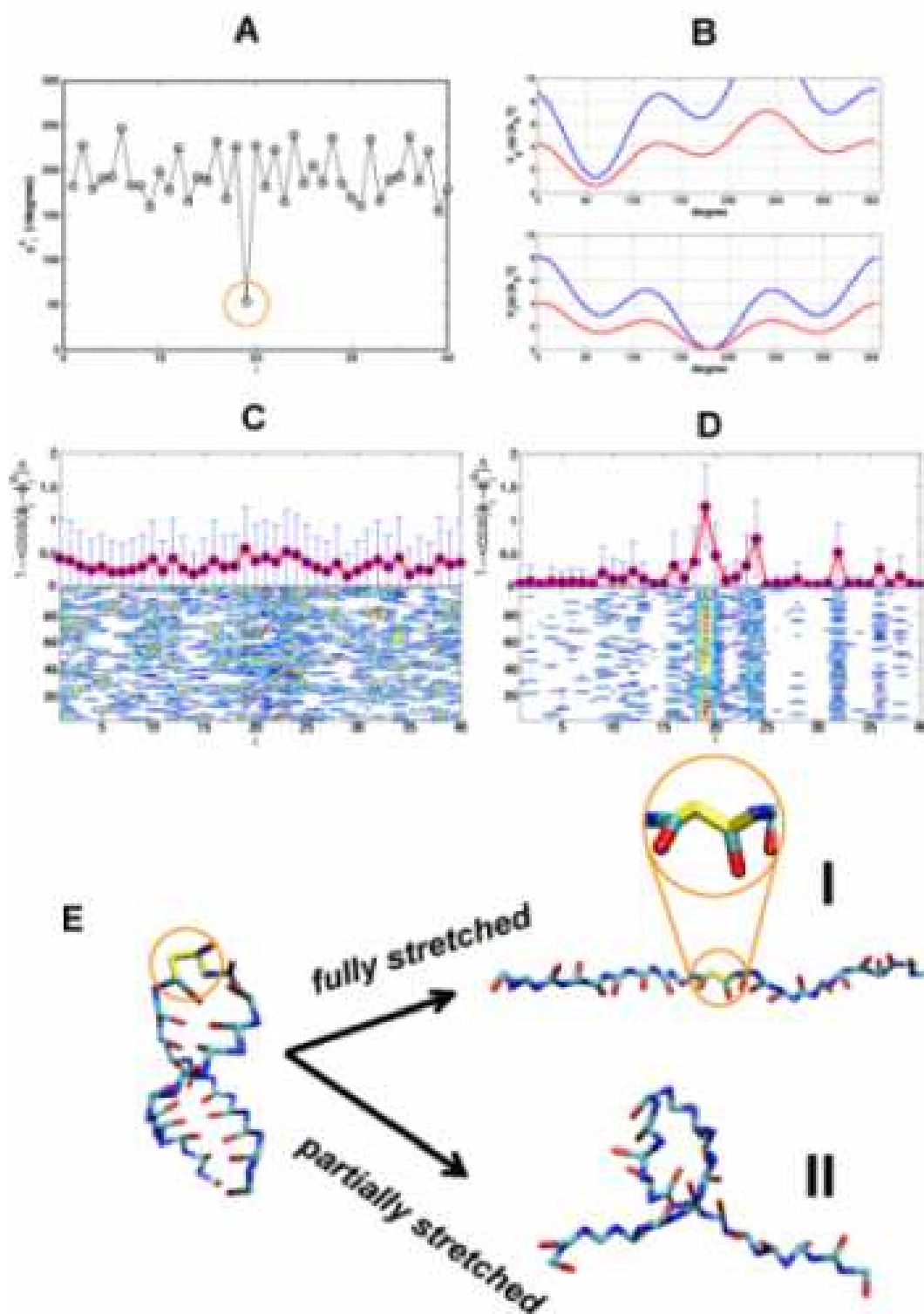


FIG. 8:

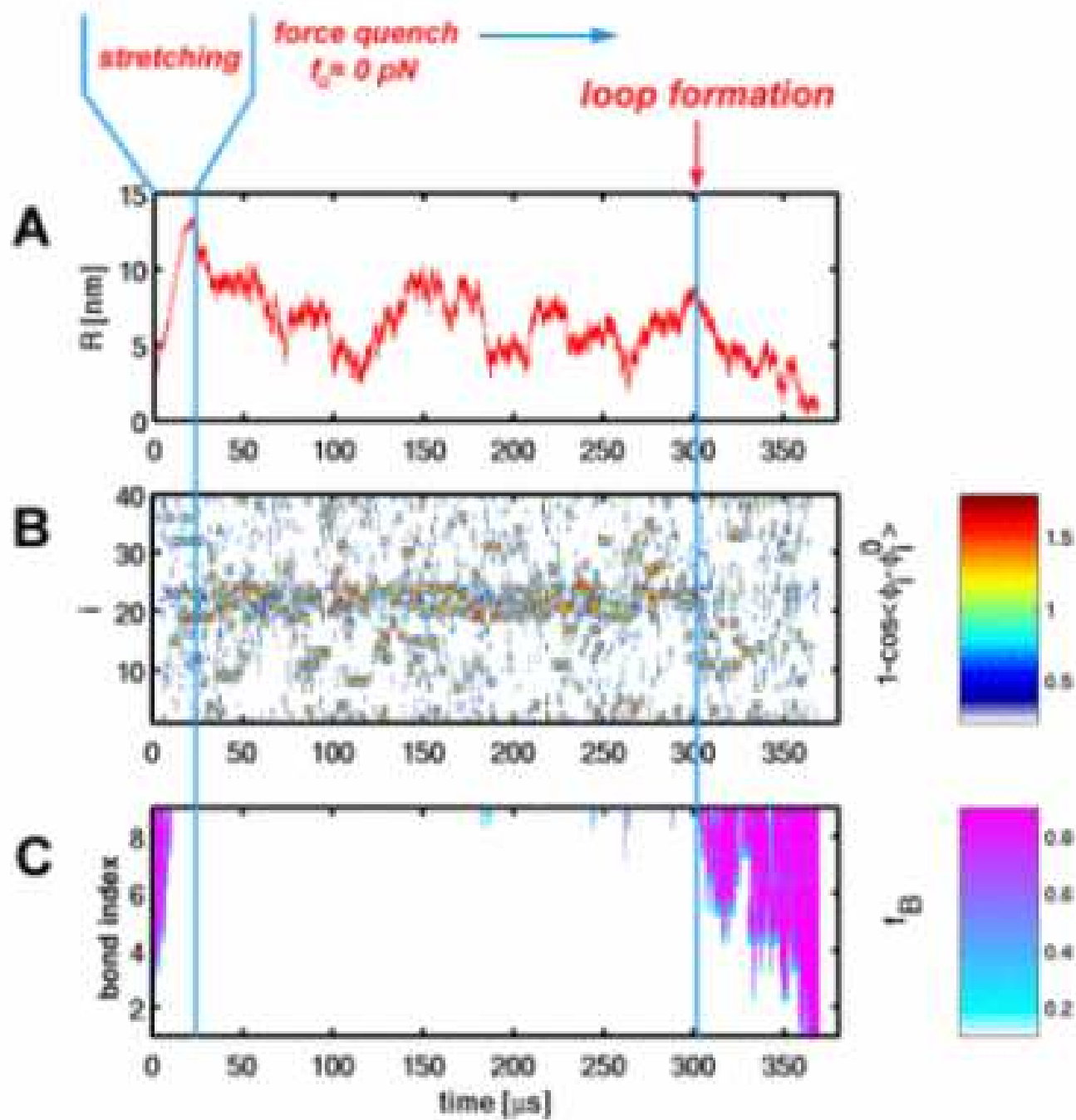


FIG. 9:

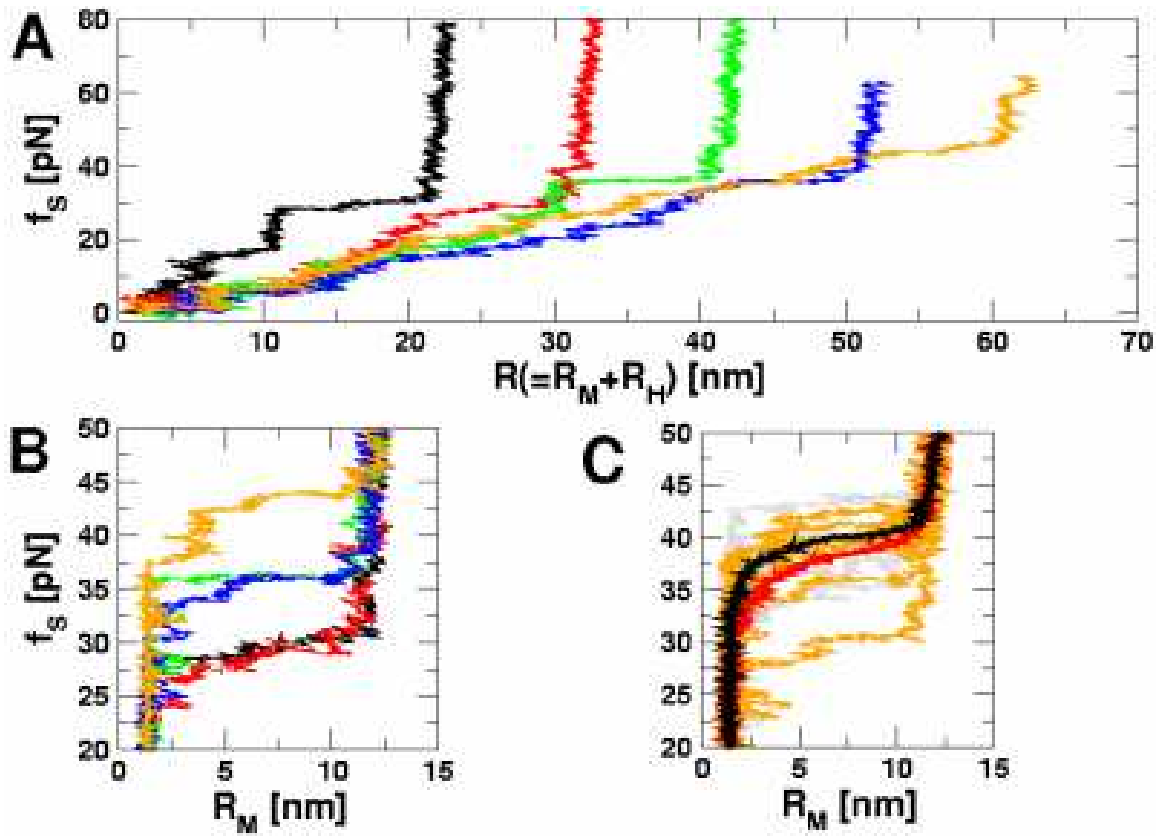


FIG. 10:

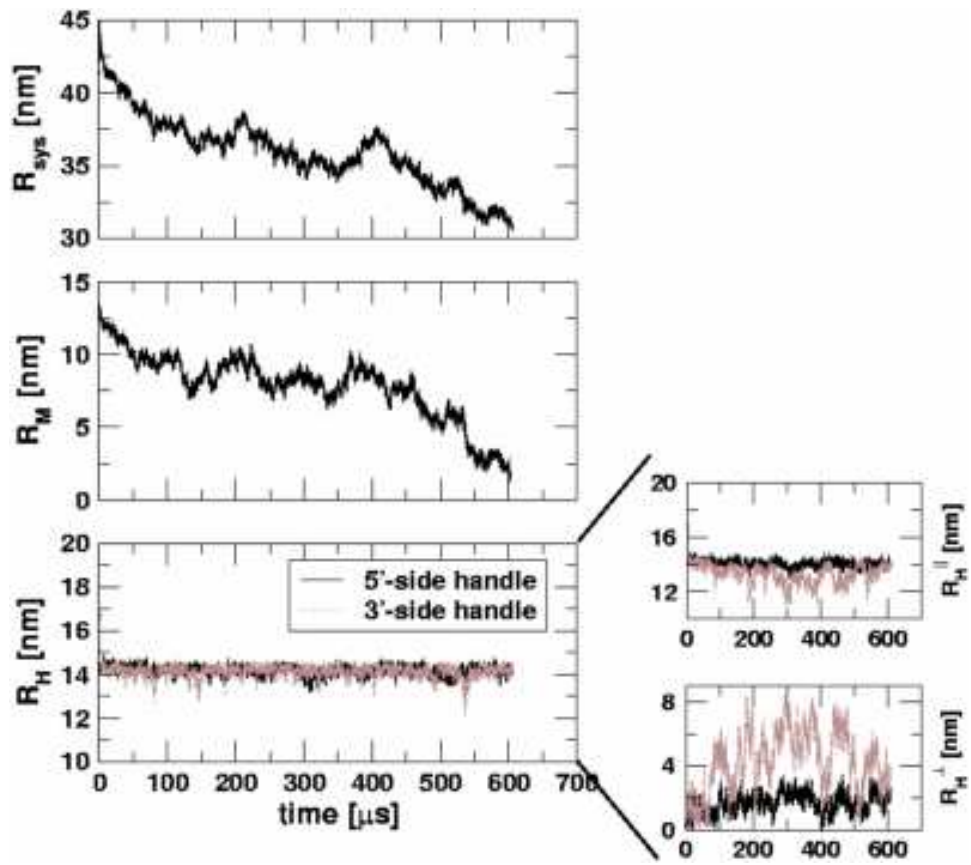


FIG. 11:

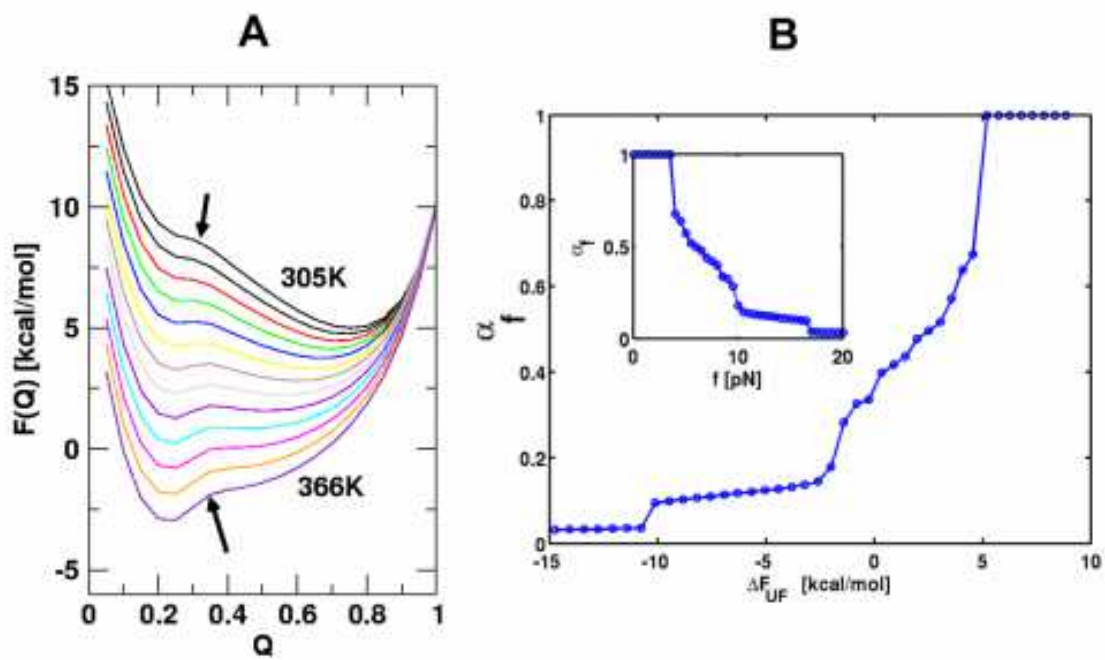


FIG. 12:

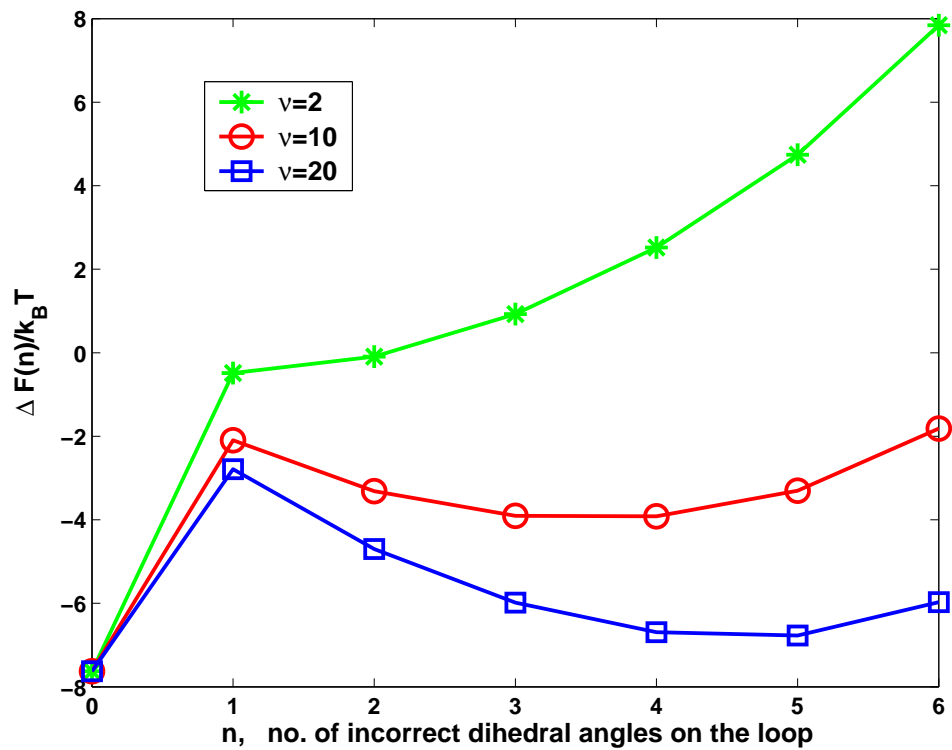


FIG. 13:

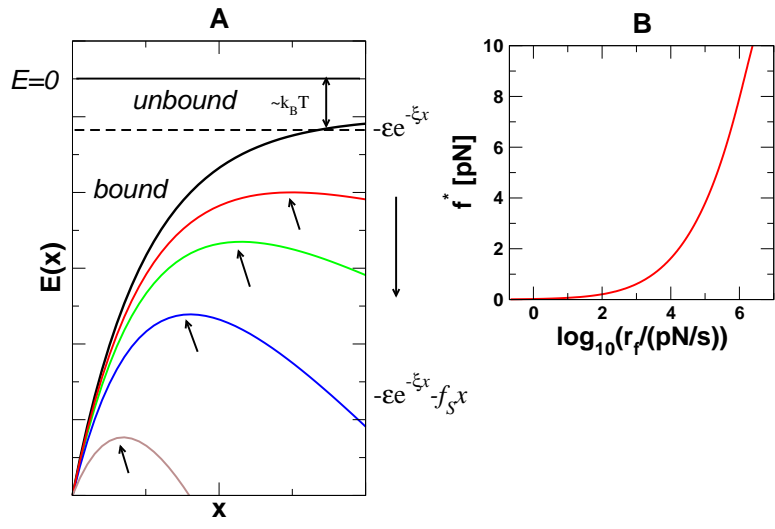


FIG. 14:

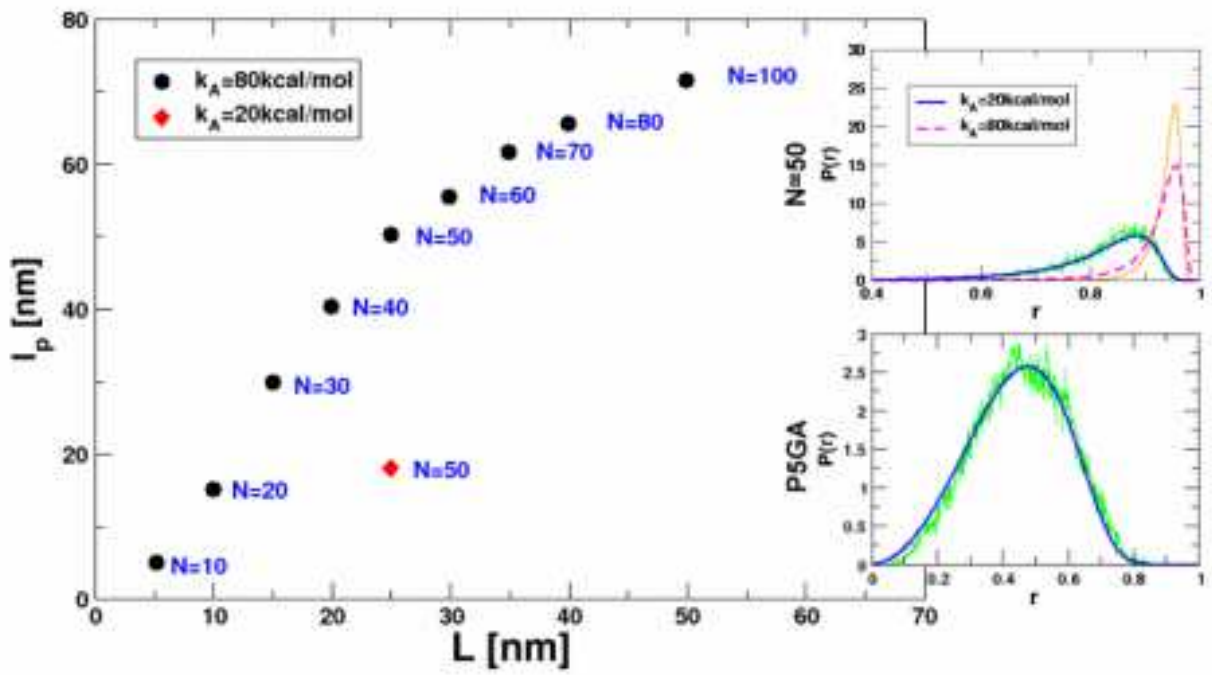


FIG. 15: